

**STRENGTH AND DEFORMABILITY OF ROCK SALT
AS AFFECTED BY CARNALLITE CONTENTS**



**A Thesis Submitted in Partial Fulfillment of the Requirements for
the Degree of Master of Engineering in Geotechnology**

Suranaree University of Technology

Academic Year 2016

ผลกระทบของแร่คาร์บอนไฟต์ต่อกำลังและการเสียรูปของเกลือหิน



วิทยานิพนธ์นี้เป็นส่วนหนึ่งของการศึกษาตามหลักสูตรปริญญาวิศวกรรมศาสตรมหาบัณฑิต

สาขาวิชาเทคโนโลยีธรณี

มหาวิทยาลัยเทคโนโลยีสุรนารี

ปีการศึกษา 2559

**STRENGTH AND DEFORMABILITY OF ROCK SALT AS
AFFECTED BY CARNALLITE CONTENTS**

Suranaree University of Technology has approved this thesis submitted in partial fulfillment of the requirements for a Master's Degree.

Thesis Examining Committee

(Assoc.Prof.Dr.PornkasemJongpradist)

Chairperson

(Asst. Prof. Dr. DechoPhueakphum)

Member (Thesis Advisor)

(Prof. Dr. KittitepFuenkajorn)

Member

(Prof. Dr. SukitLimpijumnong)

Vice Rector for Academic Affairs
and Innovation

(Assoc. Prof. Flt. Lt. Dr. KontornChamnprasart)

Dean of Institute of Engineering

อมรรัตน์ หลวงทิพย์: ผลกระทบของแร่คาร์เนลไลต์ต่อกำลังและการเสียรูปของเกลือหิน
(STRENGTH AND DEFORMABILITY OF ROCK SALT AS AFFECTED
BY CARNALLITE CONTENTS) อาจารย์ที่ปรึกษา:ผู้ช่วยศาสตราจารย์ ดร.เดโช
เผือกภูมิ, 87หน้า.

วัตถุประสงค์ของการศึกษา นี้คือเพื่อศึกษาเสถียรภาพเชิงกลศาสตร์ของเสาค้ำยันในเมือง
โพแทชที่ขุดเจาะในหมวดหินซุคมหาสารคามในภาคตะวันออกเฉียงเหนือของประเทศไทย ตัวอย่าง
หินที่มีปริมาณ แร่คาร์เนลไลต์ เจือปนตั้งแต่ 0 ถึง 100เปอร์เซ็นต์มีการทดสอบใน
ห้องปฏิบัติการเพื่อศึกษาคุณสมบัติเชิงกลศาสตร์ ผลการทดสอบระบุว่า ค่ากำลังรับแรงกด ค่ากำลัง
รับแรงดึงและค่าสัมประสิทธิ์ความยืดหยุ่นของตัวอย่างหิน มีค่าลดลงแบบเอกซ์โพเนนเชียล เมื่อ
ปริมาณการเจือปน ของแร่คาร์เนลไลต์เพิ่มขึ้นผลกระทบของปริมาณแร่คาร์เนลไลต์ ต่อการ
เปลี่ยนแปลงของคุณสมบัติเชิงกลศาสตร์เหมือนกันในทุกระดับความเค้นล้อมรอบที่ใช้ในการศึกษา
นี้ (1-12 เมกะปาสกาล) สัดส่วนการขุดเจาะมีค่าลดลงเมื่อปริมาณการเจือปนของแร่คาร์เนลไลต์และ
ระดับความลึก ของช่องเหมือง เพิ่มขึ้นเนื่องจาก แร่คาร์เนลไลต์ ประกอบด้วย แร่ซิลิเกตร้อยละ 26.8
โดยน้ำหนักเมื่อมีปริมาณการเจือปน ของแร่คาร์เนลไลต์เพิ่มขึ้น ส่งผลให้ค่าความแข็งของเสาค้ำยัน
และสัดส่วนการขุดเจาะแรลดลง แต่จะให้การขุดเจาะได้แร่ซิลิเกตที่มีความเข้มข้น สูงขึ้น เกณฑ์การ
แตกที่ถูกพัฒนาขึ้นในการศึกษานี้ สามารถนำมาอธิบายและแสดงถึง ขอบเขต ที่มีการเปลี่ยนแปลง
รูปร่างและบริเวณที่เกิดการพัง ของเกลือหินบริเวณ รอบหลุมเจาะ ขอบเขตของความไม่มีเสถียรภาพ
มีค่าเพิ่มขึ้นเมื่อการเจือปนของแร่คาร์เนลไลต์และระดับความลึกเพิ่มขึ้น

สาขาวิชาเทคโนโลยีธรณี ลายมือชื่อนักศึกษา
ปีการศึกษา 2559 ลายมือชื่ออาจารย์ที่ปรึกษา

AMORN RAT LUANGTHIP: STRENGTH AND DEFORMABILITY OF
ROCK SALT AS AFFECTED BY CARNALLITE CONTENTS.

THESIS ADVISOR: ASST. PROF. DECHO PHUEAKPHUM, Ph.D., 87 PP.

SALT/DILATION/STRENGTH/STRENGTH CRITERION

The objective of this study is to determine the mechanical stability of support pillars in potash mines openings excavated in the MahaSarakham formation. Mechanical characterization tests have been performed on the potash specimens with carnallite contents ($C_{\%}$) varying from 0% to 100%. The compressive and tensile strengths and elastic moduli of the specimens exponentially decrease with increasing $C_{\%}$. The effects of the carnallite contents tend to act equally throughout the range of the confining pressures used here (0-12 MPa). The extraction ratios decrease with increasing $C_{\%}$ and depth. Since the carnallite contains 26.8% by weight of sylvite (KCl), when $C_{\%}$ increases, the pillar strength and extraction ratio decrease, but the excavated rock contains higher concentration of KCl. The strength criteria are derived as a function of $C_{\%}$ and used to determine the extents of dilation and failure zones in rock salt around circular opening. The thickness of these zones increases with depth and $C_{\%}$.

Academic Year 2016

Advisor's Signature _____



ACKNOWLEDGMENTS

I wish to acknowledge the funding supported by Suranaree University of Technology (SUT).

I would like to express my sincere thanks to Prof. Dr. Kittitep Fuenkajorn for his valuable guidance and efficient supervision. I appreciate his strong support, encouragement, suggestions and comments during the research period. My heartfelt thanks to Assoc. Prof. Dr. Pornkasem Jongpradist, Asst. Prof. Dr. Decho Phueakphum and Dr. Prachya Tepnarong for their constructive advice, valuable suggestions and comments on my research works as thesis committee members. Grateful thanks are given to all staffs of Geomechanics Research Unit, Institute of Engineering who supported my work.

Finally, I would like to thank beloved parents for their love, support and encouragement.

Amornrat Luangthip

TABLE OF CONTENTS

	Page
ABSTRACT (THAI).....	I
ABSTRACT (ENGLISH).....	II
ACKNOWLEDGEMENTS	III
TABLE OF CONTENTS	IV
LIST OF TABLES	VIII
LIST OF FIGURES	IX
SYMBOLS AND ABBREVIATIONS	XIII
CHAPTER	
I INTRODUCTION	1
1.1 Background and rationale	1
1.2 Research objectives.....	3
1.3 Research methodology.....	3
1.3.1 Literature review	4
1.3.2 Sample preparation.....	4
1.3.3 Laboratory test.....	4
1.3.4 Analysis and assessment	6
1.3.5 Potential applications	6
1.3.6 Discussions and conclusions.....	6
1.3.7 Thesis writing and presentation	6

TABLE OF CONTENTS(Continued)

	Page
1.4 Scope and limitations	6
1.5 Thesis contents	7
II LITERATURE REVIEW	8
2.1 Introduction	8
2.2 Basic properties of rock salt	8
2.2 Strength criteria	13
2.3 Extraction ratio	20
2.4 Borehole Stability	21
III SAMPLE PREPARATION	23
3.1 Sample preparation	23
3.2 Chemical composition	24
IV LABORATORY TESTING	26
4.1 Introduction	26
4.2 Brazilian tension test	26
4.3 Uniaxial compression test	26
4.4 Point load test	27
4.5 Triaxial compression tests	28
4.6 Test results	30
4.6.1 Brazilian tension test	30
4.6.2 Uniaxial compression test	31

TABLE OF CONTENTS(Continued)

	Page
4.6.3 Point load test.....	32
4.6.4 Triaxial compression tests	33
4.6.5 Elastic parameter.....	35
V STRENGTH CRITERIA.....	42
5.1 Introduction.....	42
5.2 Strength criteria	42
5.3 Strength criterion based on strain energy principle.....	48
VI PILLAR STABILITY	50
6.1 Introduction.....	50
6.2 Extraction ratio	50
VII SHAFT STABILITY.....	57
7.1 Introduction.....	57
7.2 Shaft stability.....	57
VIII DISCUSSIONS, CONCLUSIONS AND RECOMMENDATIONS FOR FUTURE STUDIES.....	65
8.1 Discussions	65
8.2 Conclusions.....	66
8.3 Recommendations for future studies	68
REFERENCES	69
APPENDIX A SUMMARIZES DIMENSIONS OF THE SPECIMEN.....	75

TABLE OF CONTENTS(Continued)

	Page
BIOGRAPHY.....	87



LIST OF TABLES

Table	Page
2.1	Crystallographic data calculated at the GGA/PBE level of theory.....13
2.2	Comparison of Brazilian tensile strengths, uniaxial compressive strengths, elastic modulus and Poisson's ratio of salt from various sources.....14
2.3	Comparison of cohesion and Internal friction angles of salt from various sources.....16
3.1	Chemical compositions of some specimens.....25
4.1	Summary of the strength results and Elastic parameters obtained from triaxial compression tests.....38

LIST OF FIGURES

Figure	Page
1.1	Research Methodology5
2.1	Comparison of estimated bulk density from mineralogical result of measured bulk density for test specimens10
2.2	Crystal unit cells of carnallite ($\text{KCl}\cdot\text{MgCl}_2\cdot 6\text{H}_2\text{O}$; Pnna; $Z = 12$) optimized at the GGA/PBE level of theory.11
3.1	Some specimens prepared for the laboratory test.....25
4.1	Rock salt specimen with diameter placed under uniaxial load frame27
4.2	Rock salt specimen with diameters of $54\times 54\times 108$ mm placed under uniaxial load frame28
4.3	Point load testing on rock salt specimen.....28
4.4	Polyaxial load frame used in this study29
4.5	Brazilian tensile strengths as a function of carnallite content.....31
4.6	Dilation and failure strengths as a function of carnallite content.....32
4.7	Point load strength index (a) and strength conversion factor (b) as function of carnallite content33
4.8	Stress-strain curves obtained for triaxial strength testing34
4.9	Some post-test specimens showing combination of shear failures.....35

LIST OF FIGURES (Continued)

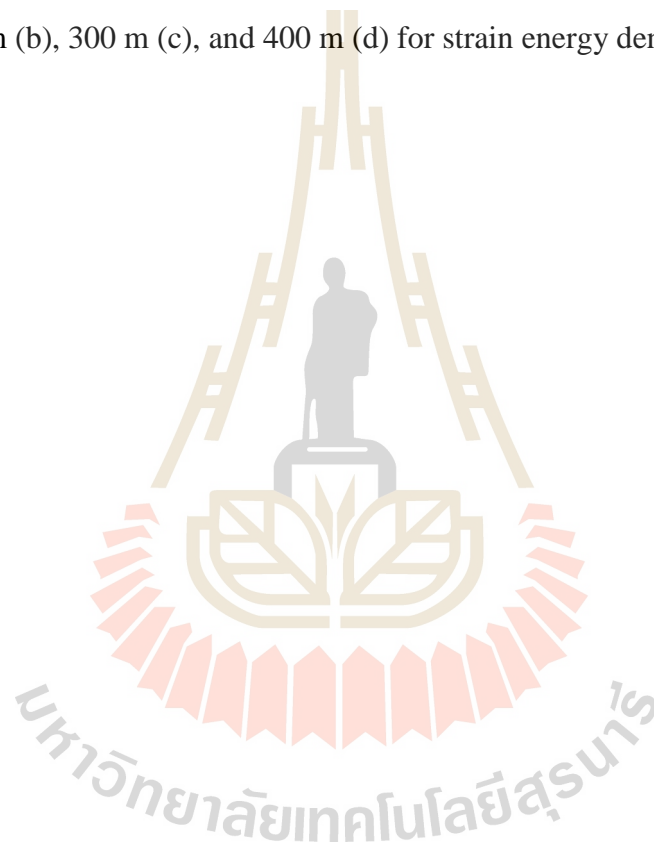
Figure	Page
4.10	Elastic modulus (a) and Poisson's ratio (b) as function of carnallite content36
5.1	Major principal stresses at dilation (a) and at failure (b) as a function of minor principal stress. Hoek-Brown strength criterion fitted to strength data. Numbers in the diagrams indicate carnallite contents44
5.2	Hoek-Brown parameter m as a function of carnallite content.....45
5.3	Major principal stresses at dilation (a) and at failure (b) as a function of minor principal stress. Yudhbir criterion fitted to strength data. Numbers in the diagrams indicate carnallite contents46
5.4	Major principal stresses at dilation (a) and at failure (b) as a function of minor principal stress. Empirical equation fitted to strength data. Numbers in the diagrams indicate carnallite contents47
5.5	Distortional strain energy at dilation ($W_{d,d}$) and at failure ($W_{d,f}$) as a function of mean stress (σ_m) for various confining pressures (σ_3) and carnallite content ($C\%$).49
6.1	Extraction ratio as a function of carnallite content ($C\%$) from Hoek and Brown criterion (a) and Yudhbir criterion (b) for various depths.....52

LIST OF FIGURES (Continued)

Figure	Page
6.2 Extraction ratio as a function of carnallite content ($C_{\%}$) from empirical equation (a) and strain energy density criteria (b) for various depths.....	53
6.3 Weigh percent of sylvite (KCl) as a function of $C_{\%}$ from Hoek and Brown criterion (a) and Yudhbir criterion (b) for various depths.....	55
6.4 Weigh percent of sylvite (KCl) as a function of $C_{\%}$ from empirical equation (a) and strain energy criterion (b) for various depths.....	56
7.1 Dilation and failure zones induced in circular opening in rock salt under various carnallite contents for depths of 100 m (a), 200 m (b), 300 m (c), and 400 m (d) for Yudhbir criterion.....	61
7.2 Dilation and failure zones induced in circular opening in rock salt under various carnallite contents for depths of 100 m (a), 200 m (b), 300 m (c), and 400 m (d) for Hoek and Brown criterion.....	62
7.3 Dilation and failure zones induced in circular opening in rock salt under various carnallite contents for depths of 100 m (a), 200 m (b), 300 m (c), and 400 m (d) for empirical equation.....	63

LIST OF FIGURES (Continued)

Figure	Page
7.4 Dilation and failure zones induced in circular opening in rock salt under various carnallite contents for depths of 100 m (a), 200 m (b), 300 m (c), and 400 m (d) for strain energy density criterion.....	64



SYMBOLS AND ABBREVIATIONS

σ_2	=	Intermediate principal stress
\AA	=	Angstrom
σ_1	=	Major principal stress
$\sigma_{1,d}$	=	Major principal stress at dilation
$\sigma_{1,f}$	=	Major principal stress at failure
σ_3	=	Minor principal stresses
σ_c	=	Uniaxial compressive strength
m	=	Hoek-Brown parameter
ν	=	Poisson's ratio
S_0	=	Shear strength or cohesion
μ_i	=	Coefficient of internal friction
τ	=	Shear strength
ϕ	=	Friction angle
σ_n	=	Normal stress
W_R	=	Room width.
W	=	Pillar width
e	=	Extraction ratio
σ_p	=	Horizontal stress
γ	=	Unit weight of rock material

SYMBOLS AND ABBREVIATIONS(Continued)

H	=	Depth
P _o	=	External pressure
σ _r	=	Radial stress
σ _θ	=	Tangential stress
τ _{oct}	=	Octahedral shear stresses
τ _{oct,f}	=	Octahedral shear stresses at failure
γ _{oct}	=	Octahedral shear strains
γ _{oct,f}	=	Octahedral shear strains at failure
∂τ _{oct} /∂t	=	Octahedral shear stresses rate
W _d	=	Distortional strain energy
W _{d,d}	=	Distortional strain energy at dilation
W _{d,f}	=	Distortional strain energy at failure
W _m	=	Mean strain energy
J ₁	=	First order of stress invariant
J ₂	=	Second order of stress invariant
a	=	Hole radial
r	=	Radial distance from the center
b	=	Empirical constant for equation (5.6, 5.7)
d	=	Empirical constant for equation (5.8, 5.9)
A	=	Empirical constant for equation (5.6, 5.7)
B	=	Empirical constant for equation (5.6, 5.7)

SYMBOLS AND ABBREVIATIONS(Continued)

C	=	Empirical constant for equation (5.8, 5.9)
D	=	Empirical constant for equation (5.8, 5.9)
ϖ	=	Empirical constant for equation (5.12)
ϖ'	=	Empirical constant for equation (5.12)
ξ'	=	Empirical constant for equation (5.12)
ξ	=	Empirical constant for equation (5.12)
ω	=	Empirical constant for equation (5.13)
ω'	=	Empirical constant for equation (5.13)
ζ	=	Empirical constant for equation (5.13)
ζ'	=	Empirical constant for equation (5.13)

CHAPTER I

INTRODUCTION

1.1 Background of problems and significance of this study

The rapid growth of resources exploitation and the potential development of underground space utilization has called for a true understanding of the mechanical behavior of the MahaSarakham rock salt, particularly those of the Middle and Lower Members. Little, however, has been known or published about the salt mechanical properties as compared to other geological data of the formation. One distinct implication is that the mechanical properties of the MahaSarakham salt tend to have high variations (Fuenkajorn, 2011). These variations may be caused by internal (intrinsic) factors (i.e., differences in grain sizes, carnallite contents, and cohesive forces between grains), and by external factors (differences in specimen sizes, loading rate, stress-paths, and testing temperature). These uncertainties have raised a question about the representation and reliability of laboratory-determined properties when applied to the design and analyses of engineering structures in salt mass.

Inclusions and impurities in salt can affect its creep deformation and strength. The degree of impurity is different for different scales. Handin et al. (1984) state that natural rock salt may contain three forms of impurities: (i) extraneous minerals may be disseminated between halite grains, (ii) some water may be trapped in the halite crystal structure or it may appear in brine filled fluid inclusions or along grain boundaries; (iii)

foreign ions such as K^+ , Ca^{2+} , Mg^{2+} , Br^- and I^- may be embedded in the crystal structure.



The coupled effects of impurities on the mechanical properties of salt can be very complicated (Franssen and Spiers, 1990; Raj and Pharr, 1992; Senseny et al., 1992). Handin et al. (1984) compare the steady-state flow parameters obtained for pure halite with those for salt samples with 0.6% MgCl_2 inclusions and with 0.1% KCl inclusions, and conclude that the inclusions appreciably affect the creep rate of salt. The quantitative effect of these inclusions, however, cannot be determined due to insufficient data. Potash has become one of the prominent ores associated with MahaSarakham salt. In the SakonNakhon basin, Asia Pacific Potash Corporation (APPC) has carried out an extensive exploration program, and drawn a detailed mine plan for extracting sylvite from the upper portion of the Lower Salt member (Crosby, 2005). It has been estimated that the inferred reserves of sylvite are about 302×10^9 t for the Udon South deposit and 665×10^9 t for the Udon North deposit. In the Khorat basin, Asean Potash Mining Company (APMC) has also conducted extensive studies and developed exploratory inclined shafts to investigate the feasibility of extracting carnallite from the Lower Salt member.

Extensive laboratory testing has been performed to determine the mechanical and rheological properties and behavior of the MahaSarakham rock salt under a variety of boundary and loading conditions. Wisetsaen et al. (2015) suggests that the tensile elastic modulus of the salt linearly decreases with increasing temperature. The salt specimens also exhibit time-dependent behavior under tension, particularly under high temperatures and low loading rates. Fuenkajorn et al. (2012) conclude from their experimental results that the salt elasticity and compressive strength increase with the loading rates. The strains induced at failure decrease as the loading rate increases. Sriapai et al. (2013) find that the intermediate principal stress (σ_2) or Lode parameter

can affect the compressive strengths of the MahaSarakham salt. The salt elasticity however tends to be independent of σ_2 .

The researches above concentrate their efforts on the properties and behavior of rock salt with virtually pure halite. The effects of carnallite content on the mechanical and rheological properties have never been addressed and investigated. Such knowledge can improve the understanding of the creep flowage and existing structures of the in-situ salt and carnallite. It is also important for the carnallite ore exploitation and excavation design in the basins.

The objective of this study is to determine the effects of carnallite contents on the strength and elasticity of the MahaSarakham rock salt. The effort involves characterization testing of the rock salt specimens with various carnallite contents. Uniaxial and triaxial compression tests are performed to determine the elastic parameters and compressive strengths of the specimens. The tensile strengths are investigated by performing the Brazilian tension test. Hoek-Brown criterion is derived as a function of carnallite contents to determine the extents of dilation and failure zones in rock salt around vertical shaft. The minimum lining strength and thickness are calculated based on the strain energy density principle.

1.1 Research objectives

The objective of this study is to determine the effects of carnallite contents on the strength and elasticity of the MahaSarakham rock salt. The effort involves performing characterization testing of the rock salt specimens with various carnallite contents. Uniaxial and triaxial compression tests are performed to determine the elastic parameters and compressive strengths of the rocks. The tensile strengths are

investigated by performing the Brazilian tension test. The modes of failure and deformations of the specimens are identified and discussed. Suitable strength criteria are proposed to describe the specimen failure as a function of carnallite contents and confining pressure. The effects of the carnallite contents ($C_{\%}$ percentage weight) on the borehole stability, pillar strength and extraction ratio are demonstrated.

1.3 Research methodology

The research methodology shown in Figure 1.1 comprises 7 steps; including literature review, sample preparation, laboratory test, analysis, applications, discussions and conclusions and thesis writing.

1.3.1 Literature review

Literature review is carried out to study the previous researches on the basic properties of potash, mechanical properties of salt, extraction ratio and strength criterion. The sources of information are from books, journals, technical reports and conference papers, journals, technical reports and conference papers. A summary of the literature review is given in the thesis.

1.3.2 Sample preparation

The salt and potash (Carnallite) specimens are prepared with nominal dimensions of $5.4 \times 5.4 \times 10.8 \text{ cm}^3$ for uniaxial and triaxial compression tests, and 62 mm diameter for Brazilian tensile strength and point load test. The all specimens are collected from depths ranging between 100 and 250 m at ASEAN Potash Mining Co., Ltd. (APMC) in the northeast of Thailand. The specimen belong to the MahaSarakham formation. The sample preparation and test procedures follow as

much as practical the ASTM standard practices (i.e. ASTM D3967-81, ASTM D5731-95 and ASTM D7012-07).

1.3.3 Laboratory testing

The laboratory testing includes uniaxial compression test, triaxial compression test, point load test and Brazilian tension test. The rate of the applied stress is 0.1 MPa/s for the compression test. A polyaxial load frame is used to apply lateral confining pressures of 1.7, 3, 5, 7, 9 and 12 MPa. Over 100 specimens are tested to determine the uniaxial and triaxial compressive strengths. The point load strength

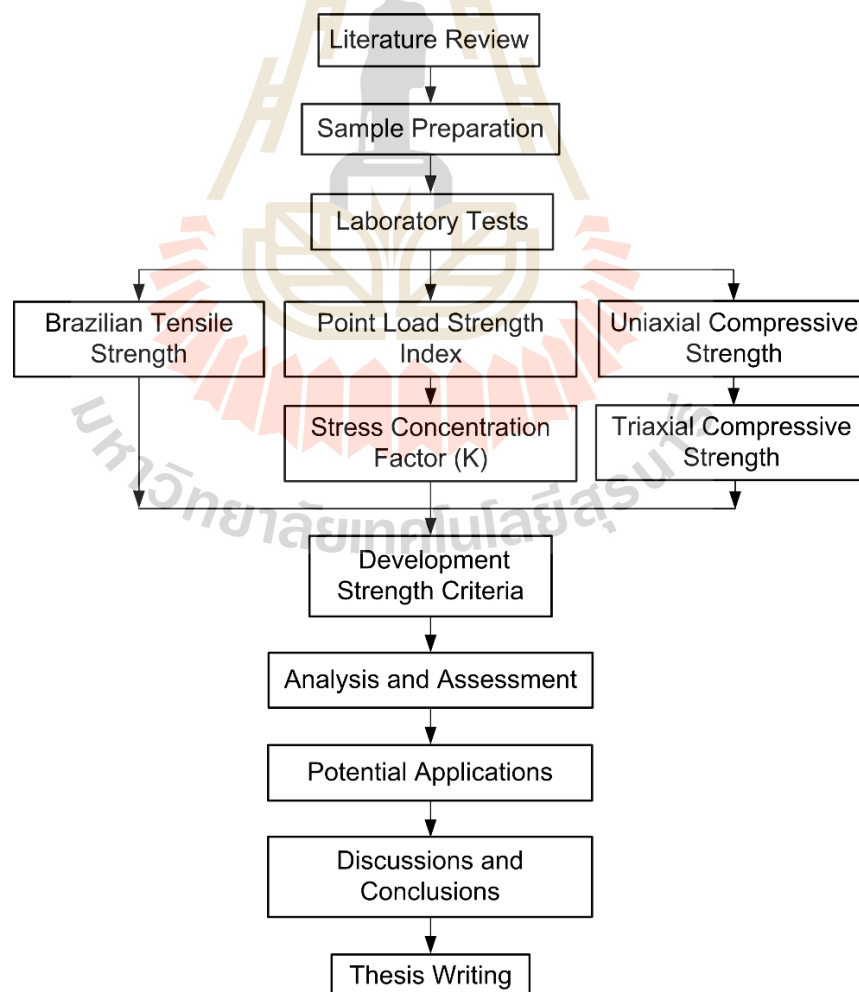


Figure 1.1 Research methodology.

index and Brazilian tension tests use over 90 specimens.

1.3.4 Analysis and assessment

Mathematical equations are derived to describe the rock strength and elasticity as a function of carnallite contents.

1.3.5 Potential applications

The obtained strength criteria are used to determine to suitable extraction ratio of salt and potash mines and to assess the stability of borehole and shaft in the formations.

1.3.6 Discussions and conclusions

Discussions are made on the reliability and adequacies of the approaches used here. Future research needs are identified.

1.3.7 Thesis writing and presentation

All research activities, methods, and results are documented and complied in the thesis. The research or findings are published in the international conference proceedings.

1.4 Scope and limitations

The scope and limitations of the research include as follows.

1. All specimens will be prepared from the MahaSarakhm formation (ASEAN Potash Mining Co., Ltd.).
2. The nominal diameters are 62 mm for Brazilian tensile strength and point load test, and $5.4 \times 5.4 \times 10.8 \text{ cm}^3$ for uniaxial and triaxial compression tests.

3. The confining pressures are maintained constant at 1.7, 3, 5, 7, 9 and 12 MPa.
4. The rate of the applied stress is 0.1 MPa/s.
5. Over 100 specimens are tested.
6. The test procedures follow the relevant ASTM standard practices, as much as practical.
7. All tests are conducted at ambient temperature.

1.5 Thesis contents

Chapter I describes the objectives, the problems and rationale, and the methodology of the research. **Chapter II** present results of the literature review of basic properties of rock salt, strength criteria, extraction ratio in salt mine and borehole stability. **Chapter III** describes the rock salt sample collection and preparation. **Chapter IV** describes the laboratory testing and test results. **Chapter V** describes the strength criteria. **Chapter VI** and **Chapter VII** describes the stability of pillar and shaft base on strength criteria. **Chapter VIII** summarizes the research results, and provides recommendations for future research studies.

CHAPTER II

LITERATURE REVIEW

2.1 Introduction

Relevant topics and previous research results are reviewed to improve an understanding of basic properties of potash and mechanical properties of salt. This review also includes the investigation of the extraction ratio and borehole stability. The summary of the results of this literature review is described below.

2.2 Basic properties of rock salt

Suwanich (2007) studies the potash-evaporite deposits in the northeastern portion of Thailand. The northeastern Thailand forms as the landscape of low elevation plateau (about 150-220 m. above mean sea level). This is called Khorat plateau. The Khorat plateau is divided into 2 basins, the north basin or SakhonNakhon basin and the south basin or Khorat basin. The potash minerals are deposited in the MahaSarakham Formation which is the rock salt main deposits. The MahaSarakham Formation is consisted of 3 layer salt beds, the Upper, Middle and Lower salt layers. These salt beds are interbedded by clastic sediments of sticky reddish brown mainly clay. The potash minerals have been found only at the top of the Lower Salt. There are only 2 kinds, carnallite ($\text{KMgCl}_3 \cdot 6\text{H}_2\text{O}$) and sylvite (KCl). They are usually deposited and interlocking with halite or rock salt grains and called the carnallitite and

sylvite strata. The other evaporate minerals mostly found in the potash minerals are tachyhydrite (Mg-

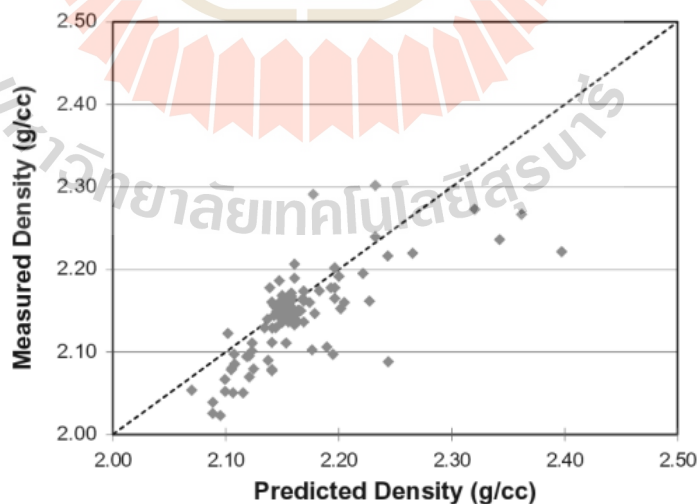


rich mineral) and rare boracites and gypsum. The structure of the MahaSarakhm Formation varies from common salt strata to salt domes. The Lower Salt is domed up through the Middle and Upper Salt closing to the surface. The peak or highest point of the domes is leached by groundwater remaining only the salt whereas the flank around the domes still remains the potash mineral containing sylvinite mainly. The carnallite is usually found beyond the flank of the domes. The theory said that the carnallite is the primary mineral while the sylvite is the secondary deposit altered from carnallite reacting with the groundwater in suitable condition.

Mellegard et al. (2012) investigate the mechanical properties of potash in the laboratory. The test specimens contained varying amounts of sylvite and carnallite. The use of X-Ray Diffraction (XRD) are costly and required destruction of the post-test sample. An alternative approach are to use the mineralogical assay result obtained by the mining company through use the X-Ray Fluorescence (XRF). Analysis of the laboratory testing data include sorting the test result into two separate databases, one for halite and one for sylvite. Initially, the shorting of the data are bases on the bulk density of each specimen that was calculated during the specimen fabrication process. The density of halite is reported as 2.16 g/cc, while the density of sylvite is reported as 1.99 g/cc (Hurlbut and Klein, 1977). Therefore, low-density specimens assumed to be high in either sylvite or carnallite, were categorized as having a density that ranged from 1.99 to 2.11 g/cc. High-density assumed to be high in halite content, were categorized as having a density that ranged from 2.12 to 2.19 g/cc. The bulk density measurements performed in the laboratory can be correlated to the mineralogical results. Using the percentage of mineral constituent, along with their respective densities, and estimated bulk density for each test specimen could be computed. A

ratio of the estimated bulk density to the measured bulk density was computed and plotted as shown in Figure 2.1. The plot in Figure 2.1 indicates that the measured bulk density values compare within ± 10 percent of the predicted density using the mineralogy result and that on average, the measured density is smaller than the predicted density, likely because the true porosity of the specimen is greater than zero.

Weck et al. (2014) reported density functional calculations of the structures and properties of carnallite ($\text{KCl}\cdot\text{MgCl}_2\cdot 6\text{H}_2\text{O}$) that possesses the orthorhombic space group *Pnna*, with $Z = 12$, and computed lattice parameters: $a = 16.28 \text{ \AA}$, $b = 22.83 \text{ \AA}$, $c = 9.59 \text{ \AA}$; $\alpha = \beta = \gamma = 90^\circ$ ($V = 3564.13 \text{ \AA}^3$; $b/a = 1.40$; $c/a = 0.59$) (Figure 2.2). The crystal structure of carnallite consists of a network of face-sharing KCl_6 octahedra and of isolated $\text{Mg}\cdot(\text{H}_2\text{O})_6$ octahedra occupying the openings in the KCl network, with the water molecules acting as charge transmitters between Mg^{2+} and Cl^- ions. The computed interatomic distances are $2.06\text{-}2.09 \text{ \AA}$ for Mg-OH_2 and $3.18\text{-}3.36 \text{ \AA}$ for K-



Cl forming

Figure 2.1 Comparison of estimated bulk density from mineralogical result of measured bulk density for test specimens. (Mellegard et al., 2012)

octahedra and the H...Cl hydrogen bonds are predicted to be in the range 2.14-2.19 Å. The computed structure is about 3.0% larger than the structure characterized by Schlemper and co-workers (Schlemper et al., 1985) using XRD (Table 2.1), with good agreement found between calculated and measured axial ratios (i.e. $b/a = 1:394$; $c/a = 0:592$). The measured interatomic distances in the octahedra are 2.027-2.053 Å for Mg-OH₂ and 3.154-3.321 Å for K-Cl and the experimental H...Cl hydrogen bonds are in the range 2.255-2.429 Å.

Tables 2.2-2.3 summarize the basic properties of rock salt from the laboratory tests from various sources.

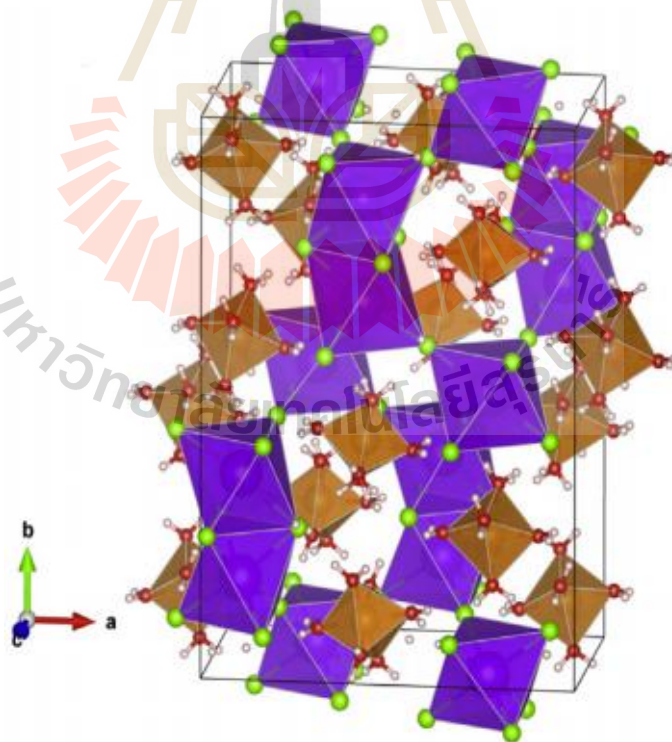


Figure 2.2 Crystal unit cells of carnallite ($\text{KCl}\cdot\text{MgCl}_2\cdot 6\text{H}_2\text{O}$; *Pnna*; $Z = 12$) optimized at the GGA/PBE level of theory. Color legend: K, purple; Ca, blue; Mg, orange; O, red; Cl, green; H, white; S, yellow. (Weck et al., 2014)

Lajtai and Duncan (1988) Specimens of potash rock from the Rocanville mine of the Potash Corporation of Saskatchewan were subjected to uniaxial compression tests and to time-dependent creep tests under static, uniaxial loading. During the first cycle of loading, the main sources of the measured strain are compaction and dilation at grain boundaries and consolidation of the clay phase. The crystals of halite and sylvite deform elastically at low stress and in a brittle manner at high stress. There is little, if any, evidence for constant-volume plastic deformation at any level of uniaxial stress. The stress-strain curve can be divided into three parts, each representing a different dominant deformational process: a low-stress quasi-elastic, an intermediate-stress ductile, and a high-stress brittle mechanism. The three parts are separated by the yield point (1-8 MPa) and the crack initiation point (10-13 MPa). The strength of the Rocanville potash specimens ranged between 15 and 18 MPa. The deformation of potash rock is strongly time dependent. There is evidence for the existence of all three stages of creep: transient, steady-state, and tertiary. There is very little interrelationship between the axial and lateral creep strains; the volumetric strain is negative at low stress and positive (dilatant) at high stress, but rarely, if ever, constant.

Schlemper et al. (1985) study unit cell and the atomic parameters of carnallite were refined from three-dimensional X-ray diffraction data ($a = 1.6119(3)$ nm, $b = 2.2472(4)$ nm, $c = 0.9551(2)$ nm, space group: *Pnna*, $Z = 12$). The structural model determining the hydrogen positions and refining anisotropic temperature coefficients.

The unique crystal structure of carnallite consists of a network of face-sharing KCl_6 octahedra and of isolated $\text{Mg}(\text{H}_2\text{O})_6$ octahedra occupying the openings in the KCl network. The water molecules act as charge transmitters between Mg^{2+} and Cl^{1-} ions.

Table 2.1 Crystallographic data calculated at the GGA/PBE level of theory.

(Hawthorne and Ferguson, 1976)

Name Sp. gp.	Carnallite <i>Pnna</i>
Z	12
a (Å)	16.28
b (Å)	22.83
c (Å)	9.59
α (°)	90
β (°)	90
γ (°)	90
V (Å ³)	3564.13

The average interatomic distances are 0.2045 and 0.3238 nm, for Mg-(H₂O) and K-Cl, respectively.

2.3 Strength criteria

The Hoek-Brown (1980) criterion defines the relationship between the major and minor principal stresses at failure as:

$$\sigma_1 = \sigma_3 + \sqrt{m\sigma_c\sigma_3 + s\sigma_c^2} \quad (2.1)$$

where σ_1 and σ_3 are the effective major and minor principal stresses, respectively, at failure; σ_c is the uniaxial compressive strength of the intact rock; m, s and a are the

strength parameters depending on the quality of the rock mass, and can be estimated by empirical expressions involving the geological strength index (GSI) and disturbance factor. Moreover, the original form of intact rock material (i.e. $s = 1$ and $a = 0.5$) has

Table 2.2 Comparison of Brazilian tensile strengths, uniaxial compressive strengths, elastic modulus and Poisson's ratio of salt from various sources. (¹Hansen et al., 1984; ²Boontongloan, 2000; ³Wetchasat, 2002; ⁴Devries et al., 2002; ⁵Jandakeaw, 2003 and ⁶Phueakhum, 2003)

Locations	Brazilian Tensile Strength (MPa)	Uniaxial Compressive Strengths (MPa)	Elastic Modulus, E (MPa)	Poisson's ratio, ν
Vacherie ¹	1.1	15.3	31.1	0.34
Petal ⁴	1.2	14.9	-	-
Avery Island	1.2	23.1	30.6	0.38
Syracuse	1.2	-	14.6	0.28
McInosh ⁴	1.3	18.1	-	0.32
Richton ¹	1.3	13.3	31.5	0.36
Mississippi Hub	1.4	-	9.5	0.31
Spindletop ⁴	1.4	22.5	-	-
Thapra, Upper Salt (DEDE)	1.4	28.4	-	-
Week's Island ¹	1.5	13.9	30.5	-
Jefferson Island ¹	1.5	24	29.5	0.29
UdonThani, Middle Salt ³	1.5	30.2	24.7	-
UdonThani, Lower Salt	1.5	31.1	28.2	0.37
Napoleonville ⁴	1.6	21.2	-	-
Trapra ⁵	1.6	29	-	0.40
New Mexico ¹	1.6	26	25.4	-
Permain ¹	1.7	22.2	26.6	0.33
Cote Blanche ¹	1.9	25.2	24.1	0.41

UdonThani, Middle Salt ⁶	1.9	30.2	-	-
UdonThani, Middle Salt ²	2.2	25.7	-	-
Paradox ¹	2.6	33.3	31.0	0.36

not been changed and is given by Hoek et al. (2002) propose a generalized form of the Hoek-Brown criterion as:

$$\sigma_1 = \sigma_3 + (m\sigma_3 \sigma_c + s\sigma_c^2)^a \quad (2.2)$$

where m is the Hoek-Brown parameter for intact rock material. The parameter m is dimensionless, and its value is affected by inter-particle friction and the degree of particle interlocking. Although it has been noted that Equation 2.2 is applicable to isotropic rocks, it may be modified to predict the failure of anisotropic intact rocks.

Coulomb criterion indicates that when shear failure takes place across a plane, the normal stress σ_n and the shear stress τ across this plane are related by functional relation characteristics of the material (Jaeger et al., 2007):

$$|\tau| = S_0 + \mu_i \sigma_n \quad (2.3)$$

where S_0 is the shear strength or cohesion of the material and μ_i is the coefficient of internal friction of the material. Since the sign of τ only affects the sliding direction, only the magnitude of τ matters. The linearized form of the Mohr failure criterion may also be written as (Jaeger et al., 2007):

$$\sigma_1 = \sigma_c + q\sigma_3 \quad (2.4)$$

$$\text{where: } q = \left[(\mu_i^2 + 1)^{1/2} + \mu_i^2 \right]^2 = \tan^2 (\pi / 4 + \phi / 2) \quad (2.5)$$

where σ_1 is the major principal effective stress at failure, σ_3 is the least principal effective stress at failure, σ_c is the uniaxial compressive strength and ϕ is the angle of

Table 2.3 Comparison of cohesion and Internal friction angles of salt from various sources. (¹Hansen et al., 1984; ²Lux and Rokahr, 1984 and ³Wetchaset, 2002)

Locations	Cohesion (MPa)	Internal friction angles (Degrees)
Vacherie ¹	2.07	59.5
Week's Island ¹	2.08	55.0
Richton ¹	2.10	51.6
S.E. New Mexico (1900' level) ¹	2.31	59.1
Avery Island ¹	2.60	-
Jefferson Island ¹	3.04	59.7
Permain ¹	3.08	56.7
Lyons ¹	3.14	-
S.E. New Mexico (2700' level) ¹	3.24	61.6
Cote Blanche ¹	3.49	58.9
Paradox ¹	4.68	58.8
Thhapra (DEDE)	5.00	49.0
UdonThani (DEDE)	6.00	49.7
Udon Thani ³	8.00	45
Gernany ²	10.00	-

internal friction equivalent to $\tan^{-1} \mu_i$. This failure criterion assumes that the intermediate principal stress has no influence on failure.

Wiebols and Cook (1968) proposed a model which describes the impact of the intermediate principal stress (σ_2) on rock strength. By considering shear strain energy of micro cracks in the rock, they gave physical description of sliding microcracks surfaces which cause failure when the stress condition meet frictional criterion. In better words, by micromechanical analysis of sliding cracks, Wiebols and Cook concluded the rock will fail when shear strain energy which is enclosed with microcracks reaches a critical level. A model which presented later on (Zhou, 1994) as an extension of circumscribed Drucker Prager is a nonlinear criterion which is called Modified Wiebols-Cook due to similarities to the original model by Wiebols and Cook (Zhou, 1994).

$$J_2^{1/2} = A + BJ_1 + CJ_1^2 \quad (2.6)$$

where J_1 is the mean effective confining stress and J_2 is the second invariant of deviatoric stress related to octahedral shear stress. The mean normal stress component in Modified Wiebols-Cook has quadratic form while in the Drucker-Prager criterion has linear form. The parameters A, B, and C can be determined from result of conventional triaxial test under different conditions. The Mohr-Coulomb criterion parameters including uniaxial compressive strength (σ_c) and flow factor (q) can be used as input for determination of A, B, and C.

$$C = \frac{\sqrt{27}}{2C_1 + (q-1)\sigma_3 - \sigma_c} \times \left(\frac{C_1 + (q-1)\sigma_3 - \sigma_c}{2C_1 + (2q+1)\sigma_3 - \sigma_c} - \frac{q-1}{q+2} \right) \quad (2.7)$$

where the coefficient of internal is frictional angle and presented.

$$C_1 = (1 + 0.6\mu_i)\sigma_c \quad (2.8)$$

σ_c is uniaxial compressive strength of the rock

$$\mu_i = \tan\phi$$

$$q = \{(\mu_i^2 + 1)^{1/2} + \mu_i\}^2 = \tan^2(\pi/4 + \phi/2)$$

And parameter A is function of B and C:

$$B = \frac{\sqrt{3}(q-1)}{q+2} - \frac{C}{3}(2\sigma_c + (q+2)\sigma_3) \quad (2.9)$$

$$A = \frac{\sigma_c}{\sqrt{3}} - \frac{\sigma_c}{3}B - \frac{\sigma_c^2}{9}C \quad (2.10)$$

The criterion can also be expressed in terms of the principal stresses at failure as:

$$\sigma_1 = \left[\frac{6(\psi - \chi) - 3(A + B\sigma_m)}{C\sigma_m} \right] - (\sigma_2 + \sigma_3) \quad (2.11)$$

where $\psi = (\sigma_1^2 + \sigma_2^2 + \sigma_3^2)$

$$\chi = (\sigma_1\sigma_2 + \sigma_1\sigma_3 + \sigma_2\sigma_3)$$

Rafai (2011) proposes a new criterion for prediction of intact rock and rock mass failure under polyaxial state of stresses. A comprehensive database of the results of uniaxial, triaxial, and polyaxial tests on the intact rock are utilized for evaluation of

the new criterion and comparison of its accuracy with the most accurate and frequently used criteria. Analysis of 195 individual data groups of brittle failure in the form of (σ_3, σ_1) for twelve different rock types showed that the proposed criterion lead to determination coefficients higher than 0.99 in most cases. It also gave the lower values of root mean squared errors relative to Mohr-Coulomb and Hoek-Brown criteria in fitting the normalized strength data for each rock type. The criteria were used to fit a typical series of triaxial strength data including brittle and ductile behavior. It showed that the new criterion can maintain its accuracy over a wider range of stresses. In the absence of rock mass strength data, the applicability of the new criterion for rock mass are verified by fitting it to typical Hoek-Brown failure envelopes. Regression analysis of the polyaxial strength data in the form of $(\sigma_3, \sigma_2, \sigma_1)$ for six rock types showed that the new criterion in all cases.

Fuenkajorn et al. (2012) proposed strain energy criterion for salt at dilation and at failure from various loading rates. Several forms of the strength and dilation criteria have been derived. It is found that the $W_{d,d}-W_{m,d}$ criterion is the most comprehensive formulation, and perhaps is the most reliable. It implicitly incorporates the rate effect, and requires complete stress-strain relations that must be obtained from compression testing under various loading rates. The $\tau_{oct,f}-\partial\tau_{oct}/\partial t$ and $\tau_{oct,d}-\partial\tau_{oct}/\partial t$ criteria are the simplest. They do not consider the induced strains, but explicitly incorporate the effects of the shear rate and mean stress into their formulation. The shear strains induced at dilation and failure are added into the formulation of the $\tau_{oct,f}-\gamma_{oct,f}$ and $\tau_{oct,d}-\gamma_{oct,d}$ criteria to implicitly consider the rate effect.

Artkhonghan and Fuenkajorn (2015) proposed energy criterion derived from constant mean stress data, which tends to give the most conservative results. The

strain energy density assumes that the stress-strain relations are linear. In reality, however, non-linear behavior has been observed for all test conditions and stress paths, in particular for the salt under large σ_3 and σ_m . As a result the strain energy determined here likely underestimates the energy that the in-situ salt can sustain before failure. This makes the application of the strain energy criterion to the stability evaluation even more conservative. The advantage of the application of the strain energy criterion over the traditional strength criteria is that it considers both shear stress and strain at failure, and hence their results would be more comprehensive than the modified Wiebols and Cook and Mogi criteria, particularly for soft and creeping rocks, such as salt, where their strains at failure are large.

2.4 Extraction ratio

The tributary area theory, also known as extraction ratio approach, is based on simple equilibrium analysis. The extraction ratio depends on the pillar layout; pillar load is calculated based on the geometry and dimension of room and pillar. For the describing pillar stress in term of extraction ratio, the following expressions modified by Biron and Arioglu (1980) can be used:

$$e = 1 - \frac{\gamma H}{\sigma_p} \quad (2.12)$$

where e is extraction ratio, σ_p is horizontal stress, γ is unit weight of rock material and H is depth.

Hedley (1967) proposed the strain is constant as the pillar height changes. This causes the convergence to change proportionally to the pillar height. The pillar height

does not affect the extraction ratio because the extraction ratio is only dependent on the area. The extraction ratio is a function of the pillar width and the room width, and it is defined by the following:

$$\text{extraction ratio} = \frac{(W + W_R)^2 - W^2}{(W + W_R)^2} = \frac{\text{excavated room area}}{\text{repository area}} \quad (2.13)$$

where W is the pillar width of a square pillar and W_R is the room width. The extraction ratio is decided based on the depth of the mine and strength of the rock salt. Most room and pillar salt mines use an extraction ratio of approximately 0.55, which is generally the most accepted economical and stable value in practice. However, there have been extraction ratios ranging from 0.20 to 0.90 for some room and pillar salt mines. Low extraction ratios are usually due to pillars widths much larger than room widths which result in low convergence rates.

2.5 Borehole Stability

Infante and Chenevert (1989) presented a mathematical and laboratory analysis that provides solutions to the problem of plastic flow of salt formations into wellbores. The predict show the salt will flow and what type of mud might be used to control such flow for various well conditions. In the mathematical analysis, it is assumed that the incipience of plasticity in the formation is regulated by the level of octahedral shear stress and that the formation is neither permeable nor porous, but homogeneous and isotropic. The stress distribution in the neighborhood of the borehole is studied, and conditions under which this distribution is elastic, elastoplastic, or plastic are determined. Equations are derived that, in terms of two

constants of the formation material, yield, and the limit of elasticity. Factors calculated include the radius of the plastic front and the percent of the borehole-diameter shrinkage as a function of mud weight used. This study was prompted by past failures in drilling through the Louann salt formation at depths of 12,500 to 14,000 ft (3810 to 4270 m), a formation that exhibits rapid plastic flow at low mud weights and at the temperatures and pressures encountered. The techniques presented were applied to subsequent drilling of this salt section, and the zone are penetrated without the problem of plastic flow. Salt-property constants were developed at elevated temperatures and pressures for the Louann salt formation by use of the triaxial test cell. Data are presented for elastic, plastic, and creep deformation of salt for pressures to 13,200 psi (91 MPa) and temperatures to 350 °F (177 °C). Nomographs are also presented to facilitate the rapid determination of salt behavior, for a given depth and temperature, it is possible to specify a mud weight so that the salt will behave either elastically, in creep flow, or plastically. If plastic flow is predicted, the amount of borehole-diameter reduction is specified.

Morita (2004) studies laboratory and field borehole stability data, an empirical correlation of borehole size and stress gradient effects is derived. Using the correlation, the well orientation effect on borehole stability is numerically studied. The study shows that the borehole stability is controlled, under the normal condition, by the largest in-situ stress in the radial borehole direction so that the borehole orientation effect for a horizontal well is not significant if two horizontal stresses are less than the vertical overburden pressure, however, if one horizontal stress is greater than the vertical stress, the orientation significantly affects the borehole stability.

CHAPTER III

SAMPLE PREPARATION

3.1 Sample preparation

Rock salt blocks ($0.5 \times 0.5 \times 0.7 \text{ m}^3$) are collected from an underground carnallite mine in the northeast of Thailand. They belong to the Lower Salt member of the MahaSarakhm formation. The carnallite beds are commonly found near the top of the Lower Salt member. Hite and Japakasetr (1979), Hite (1982) and Suwanich (1984) state that the carnallite origin should be a primary mineral and is often found near flanks or shelves of salt domes or anticlines. Only rock salt blocks that contain halite and carnallite are used to prepare the specimens in this study. The carnallite appears as crystalline or granular masses. In some blocks the interbeddings of carnallite and halite can be clearly seen. In some blocks the contacts between the two minerals cannot be defined. An attempt was made here to obtain rock cores by using an impregnated diamond coring bit with 54 mm diameter. During drilling, the high carnallite contents specimens tended to break along the bedding planes. The obtained core length was less than twice the core diameter. The specimens used for the uniaxial and triaxial compression tests are therefore prepared as rectangular blocks with nominal dimensions of $54 \times 54 \times 108 \text{ mm}^3$. Figure 3.1 shows some examples of the rectangular block specimens. For the Brazilian tension test, 62 mm diameter disks can be prepared with thickness-to-diameter ratio of 0.5.

3.2 Chemical composition

Chemical analyses by X-ray diffraction (XRD) performed on some specimens show that the primary mineral compositions of the specimens are halite and carnallite, which are of interest in this study (Table 3.1). The halite crystals are about 2-5 mm. The size of carnallite crystals varies greatly from 1 mm to 2 cm. Other minerals are relatively small and tend to appear about the same amounts in all specimens. Due to the difference of densities between halite and carnallite, the carnallite contents ($C_{\%}$) for each specimen can be estimated by:

$$C_{\%} = \left(\frac{\rho_s - \rho_c}{\rho_s - \rho_c} \right) \times 100 \quad (3.1)$$

where ρ_s is specimen density, ρ_s is density of halite (2.16 g/cc) and ρ_c is density of carnallite (1.60 g/cc) (Klein et al., 1998). The discrepancy between the carnallite contents obtained by the chemical analyses and by density ratio in equation (1) may be caused by the preparation procedure to obtain powder samples for the XRD analysis. Some hydroxyls may be lost during grinding of the rock fragments. Appendix A show summarizes the specimen number, dimensions, density and carnallite content of Brazilian tension test, uniaxial compression tests, point load test and triaxial compression tests. After preparation the specimens are wrapped with plastic sheet at all time to prevent it from subjecting to the surrounding humidity.

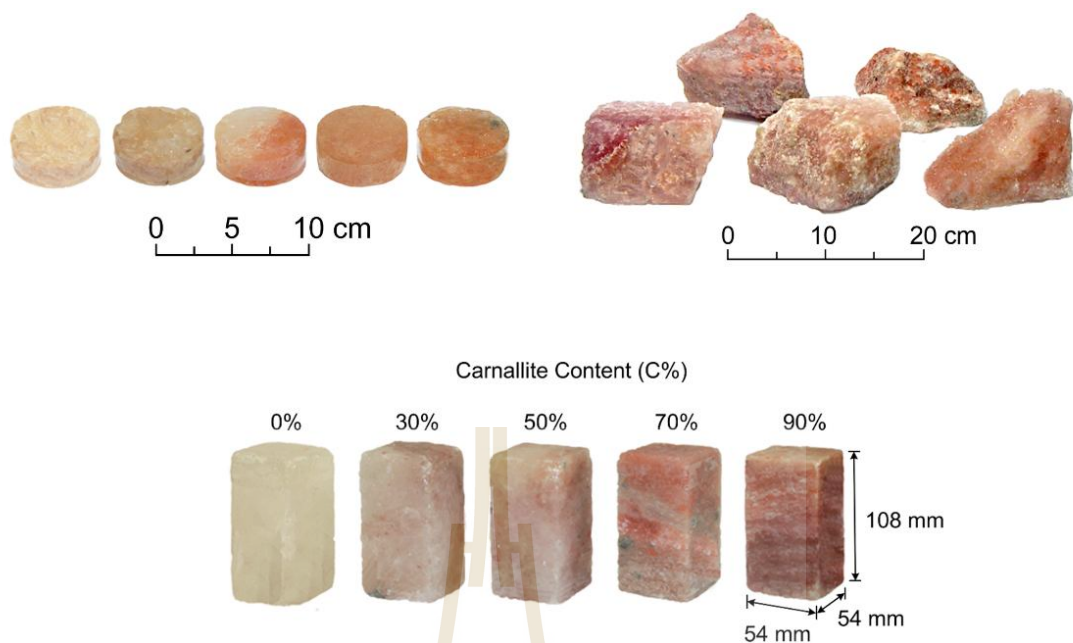
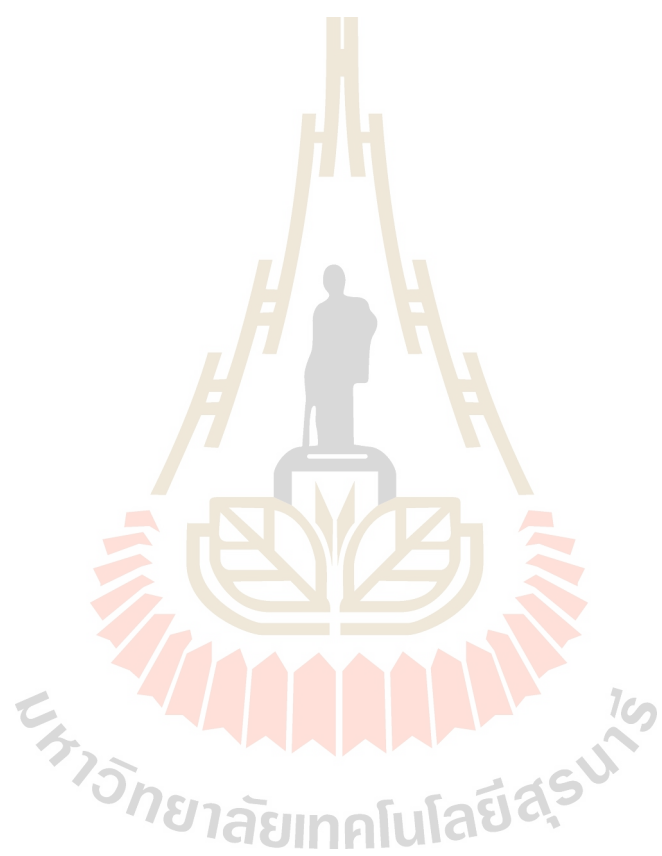


Figure 3.1 Some specimens prepared for the laboratory test.

Components	Sample no. 1	Sample no. 2	Sample no. 3	Sample no. 4
Carnallite ($\text{KMgCl}_3 \cdot 6\text{H}_2\text{O}$)	0.05	24.75	38.31	52.98
Halite (NaCl)	92.40	64.60	42.80	35.97
MgCl_2	5.71	8.93	9.69	5.55
Calcite (CaCO_3)	-	0.21	0.48	1.92
Anhydrite (CaSO_4)	0.11	0.17	0.65	1.23
Sylvite (KCl)	0.09	0.19	6.10	1.01
Hydrophilite (CaCl_2)	-	-	1.64	0.56
Wuestite	-	0.06	0.43	0.44
Calcium Chloride (CaCl)	1.65	1.08	0.89	0.33
Density (g/cc)	2.11	1.96	1.89	1.76
C% (determined by density ratio)	8.56	36.12	49.01	71.08

Table 3.1 Chemical compositions of some specimens.



CHAPTER IV

LABORATORY TESTING

4.1 Introduction

The objective of this section is to describe the test methods and results of the effects of carnallite content on strength and deformability of the MahaSarakham. All proposed testing procedures and equipment are also described.

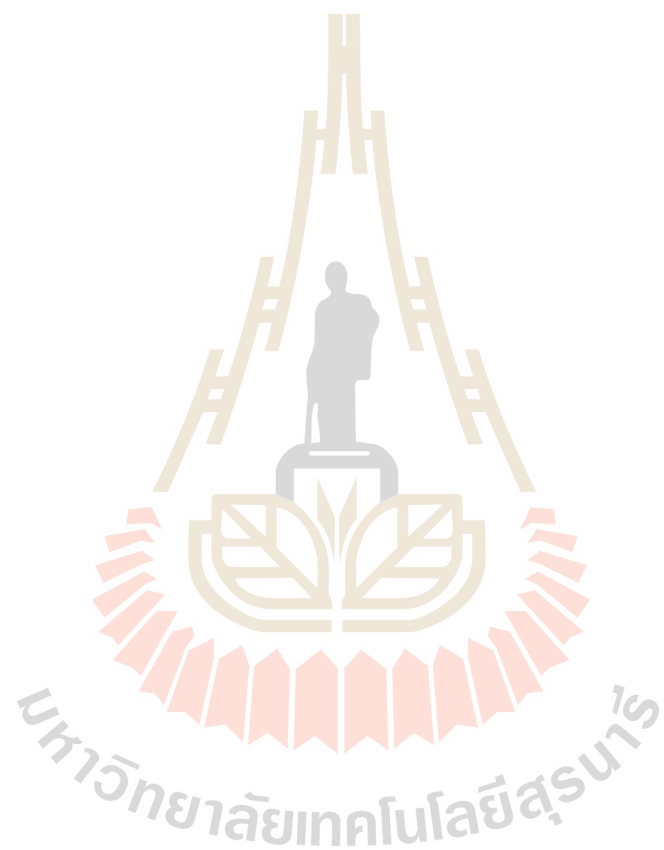
4.2 Brazilian tension test

The Brazilian tension test method and calculation follow the ASTM (D3967-81) standard practice and the ISRM suggested methods (Brown, 1981). Over sixty specimens with various carnallite contents have been tested. The specimens have nominal diameters of 54 mm with length-to-diameter of 0.5. The bedding planes are parallel to the specimen axis (Figure 4.1).

4.3 Uniaxial compression test

The objective of the uniaxial compression tests is to determine the ultimate strength and the deformability of the specimens under uniaxial load at various carnallite content. The test procedures follow the American Society for Testing and Materials (ASTM D 7012-07) and the suggested methods by ISRM (Bieniawski and

Bernede, 1978). The tests are performed by applying uniform axial stress
underconstant rate at



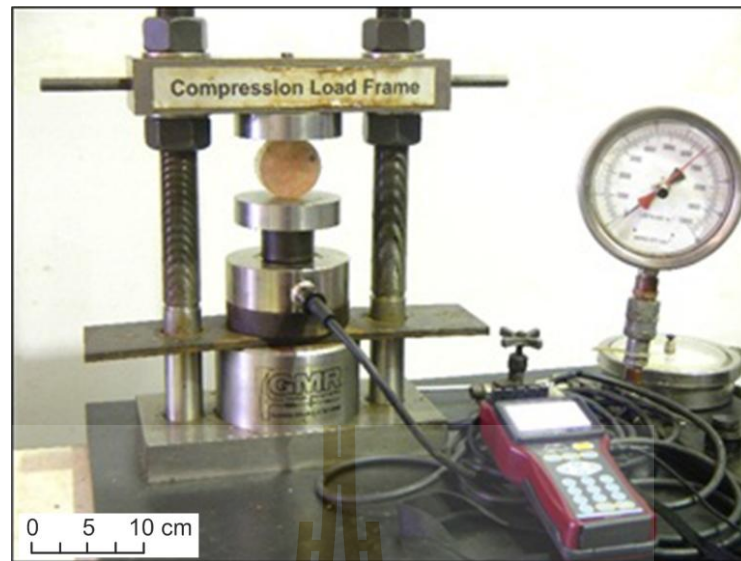


Figure 4.1 Rock salt specimen with diameter placed under uniaxial load frame.

0.1 MPa/s to the rectangular rock specimen and measuring the increase of axial strains as a function of time (Figure 4.2). The post-failure characteristics are observed and recorded.

4.4 Point Load Test

The point load strength test is performed using irregular shaped specimens with nominal dimensions of 10-20 cm. The test method follows the ASTM (D5731-95) standard practice. Over fifty specimens have been tested. The loading direction is normal to the bedding planes whenever they can be defined (Figure 4.3)

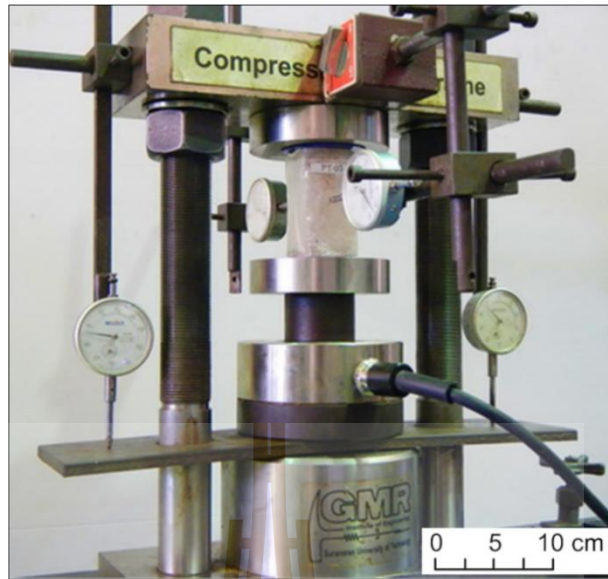


Figure 4.2 Rock salt specimen with dimensions of $54 \times 54 \times 108 \text{ mm}^3$ placed under uniaxial load frame.

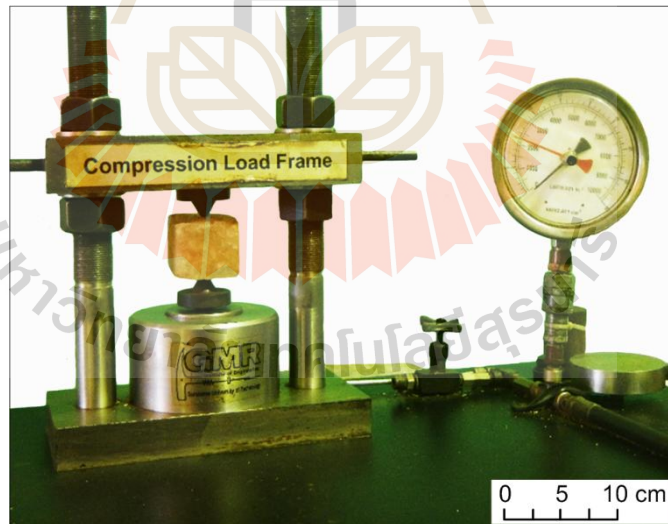


Figure 4.3 Point load testing on rock salt specimen.

4.5 Triaxial compression tests

A polyaxial load frame (Figure 4.4) has been used to apply lateral and axial stresses on the rectangular specimens. Sixty specimens have been tested. Except for the specimen geometry the test procedure and calculation follow the ASTM (D7012-07) standard practice. Exhaustive reviews of the polyaxial load frame have recently been

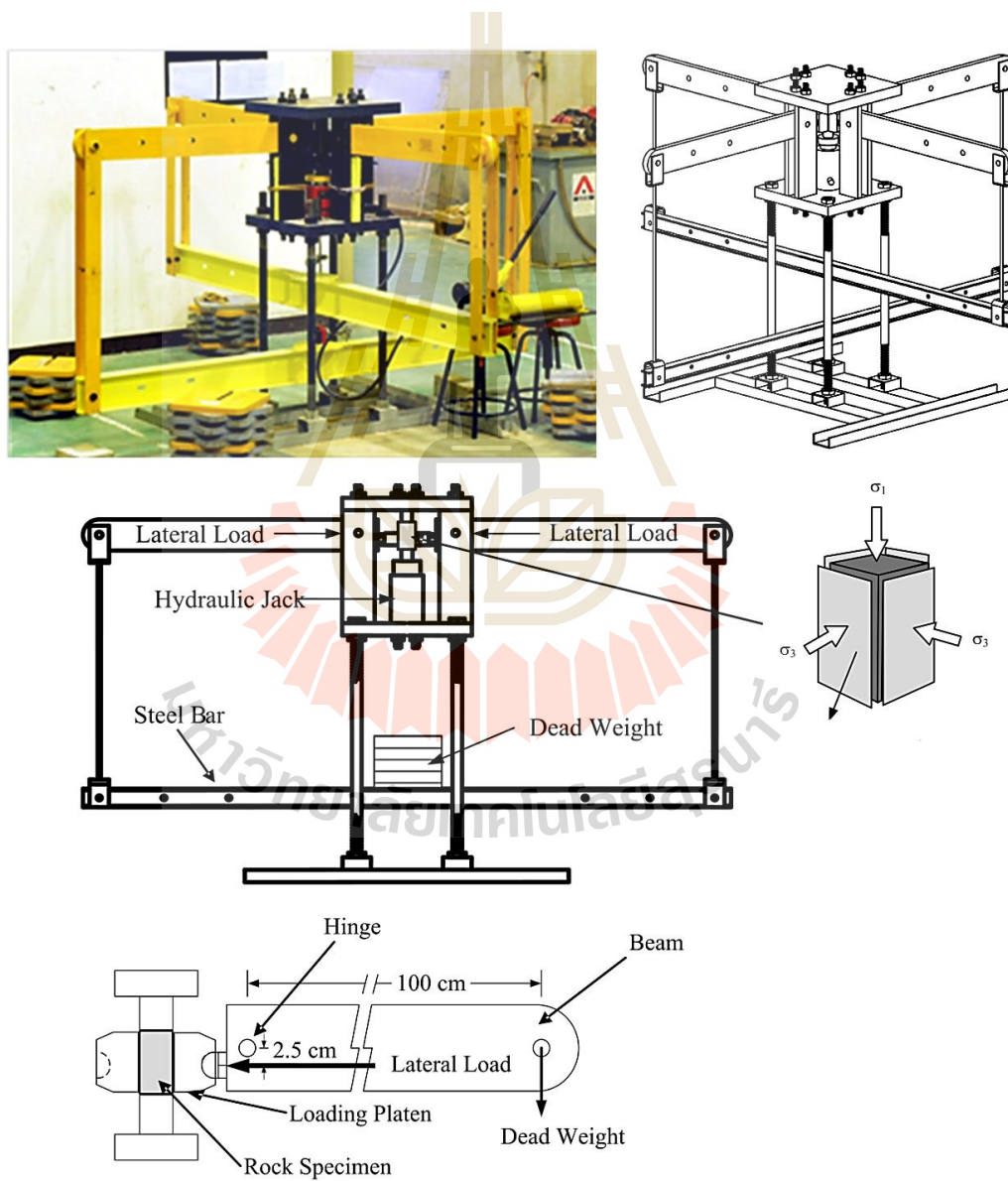


Figure 4.4 Polyaxial load frame used in this study (Walsri et al., 2009).

given in Fuenkajorn et al. (2012). The testing system is always calibrated before testing. In this study, σ_2 and σ_3 are equal ranging from 1.7, 3, 5, 7, 9, 12 MPa. Perforated neoprene sheets have been placed at the interface between loading platens and rock surfaces to minimize the friction for saturated condition. After installing the rectangular specimen into the load frame, dead weights are placed on the steel bar to obtain the pre-defined magnitude of the uniform lateral stress (σ_3) on the specimen. The test is started by increasing the vertical stress at the predefined rate using the hydraulic pump. Both the axial strain and lateral strain were properly recorded directly by a dial gage during the testing. The failure stresses are recorded and mode of failure examined.

4.6 Test results

4.6.1 Brazilian tension test

Figure 4.5 plots the Brazilian tensile strengths (σ_B) as a function of $C_{\%}$ varying from 0% (pure halite) to 94%. Post-test observations show that there are two combined modes of fracturing in the specimens: cleavage fracturing in halite and conchoidal fracturing in carnallite. The tensile strengths decrease exponentially with increasing carnallite contents:

$$\sigma_B = 1.88 \cdot \exp(-0.020 \cdot C_{\%}) \quad \text{MPa} \quad (4.1)$$

The tensile strengths for pure carnallite specimens are about 14% of those of pure halite. The strengths show relatively high intrinsic variability ($R^2 = 0.873$) for all $C_{\%}$'s. This could be explained by the fact that the tensile splitting of the disk

specimen may be governed by the orientations and amounts of halite and carnallite along the

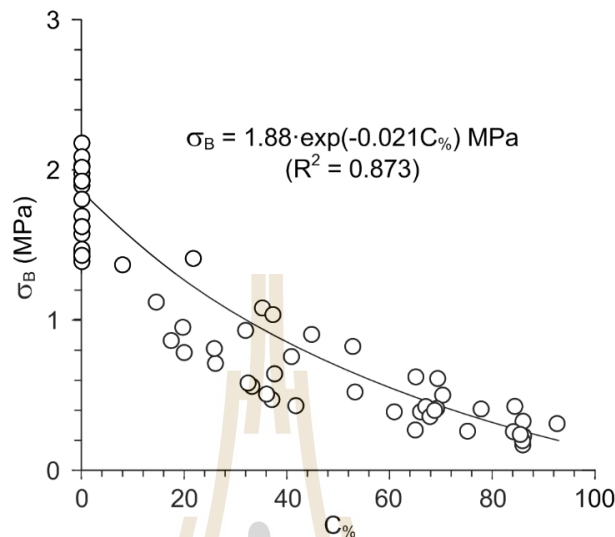


Figure 4.5 Brazilian tensile strengths as a function of carnallite content.

loading diameters. Under the same $C\%$, the specimens may show high strengths if the tensile splitting occurs through salt crystals. The low strengths may be obtained for the tensile cracks that are largely induced through the carnallite crystals.

4.6.2 Uniaxial compression test

The uniaxial compressive strengths (σ_c) as a function of $C\%$ at dilation and at failure are shown in Figure 4.6. The dilation strength is the point at which the specimen is loaded and deformed to its elastic limit. Beyond this point the microcracks are initiated, the specimen volume increases, and the axial stress-strain relation is no longer linear. The results show that the strengths at dilation ($\sigma_{c,d}$) and at failure ($\sigma_{c,f}$) exponentially decrease with increasing $C\%$, and can be represented by:

$$\sigma_{c,d} = 8.89 \cdot \exp(-0.021 \cdot C\%) \quad \text{MPa} \quad (4.2)$$

$$\sigma_{c,f} = 23.19 \cdot \exp(-0.012 \cdot C\%) \quad \text{MPa} \quad (4.3)$$

The exponential equations above fit relatively well to the strength results ($R^2 > 0.8$). The dilation strength is about 40% of the failure strength for rock salt specimens with pure halite ($C\% = 0$), and about 10% of the failure strength for specimens with over 80% carnallite content. Shear fractures are induced in all specimens. They cut through both halite and carnallite crystals. No distinctive difference of the failure mode is found among specimens with different $C\%$.

4.6.3 Point load test

The relations between the point load strength index (I_s) and $C\%$ are shown in Figure 4.7(a). Mode of failure shows extensile splitting between the loading points. The point load strength index (I_s) exponentially decreases with increasing $C\%$:

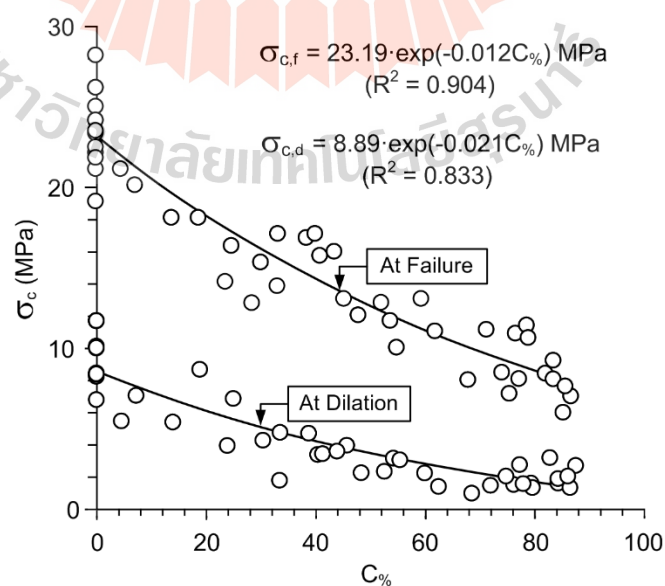


Figure 4.6 Dilation and failure strengths as a function of carnallite content.

$$I_s = 1.77 \cdot \exp(-0.011 \cdot C_{\%}) \quad \text{MPa} \quad (4.4)$$

The stress conversion factor (k) between σ_c and I_s for various carnallite contents can be determined. The values of k slightly decrease with increasing $C_{\%}$ (Figure 4.7(b)) and can be represented by:

$$k = (\sigma_c / I_s) = -0.013 \cdot C_{\%} + 13.091 \quad (4.5)$$

4.6.4 Triaxial compression tests

Figure 4.8 shows the stress-strain curves monitored from the triaxial test specimens under various carnallite contents and confining pressures. The effect of carnallite contents can be observed by the reduction of failure stresses, and the increase

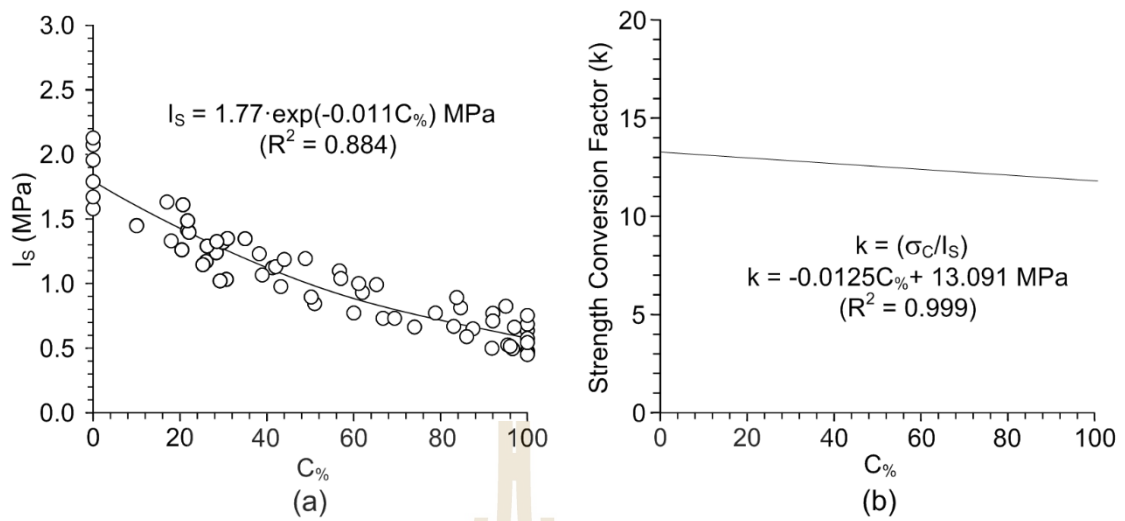


Figure 4.7 Point load strength index (a) and strength conversion factor (b) as function of carnallite content.

of the failure strains, particularly under low confining pressures. All post-test specimens show multiple shear failures shown in Figure 4.9.

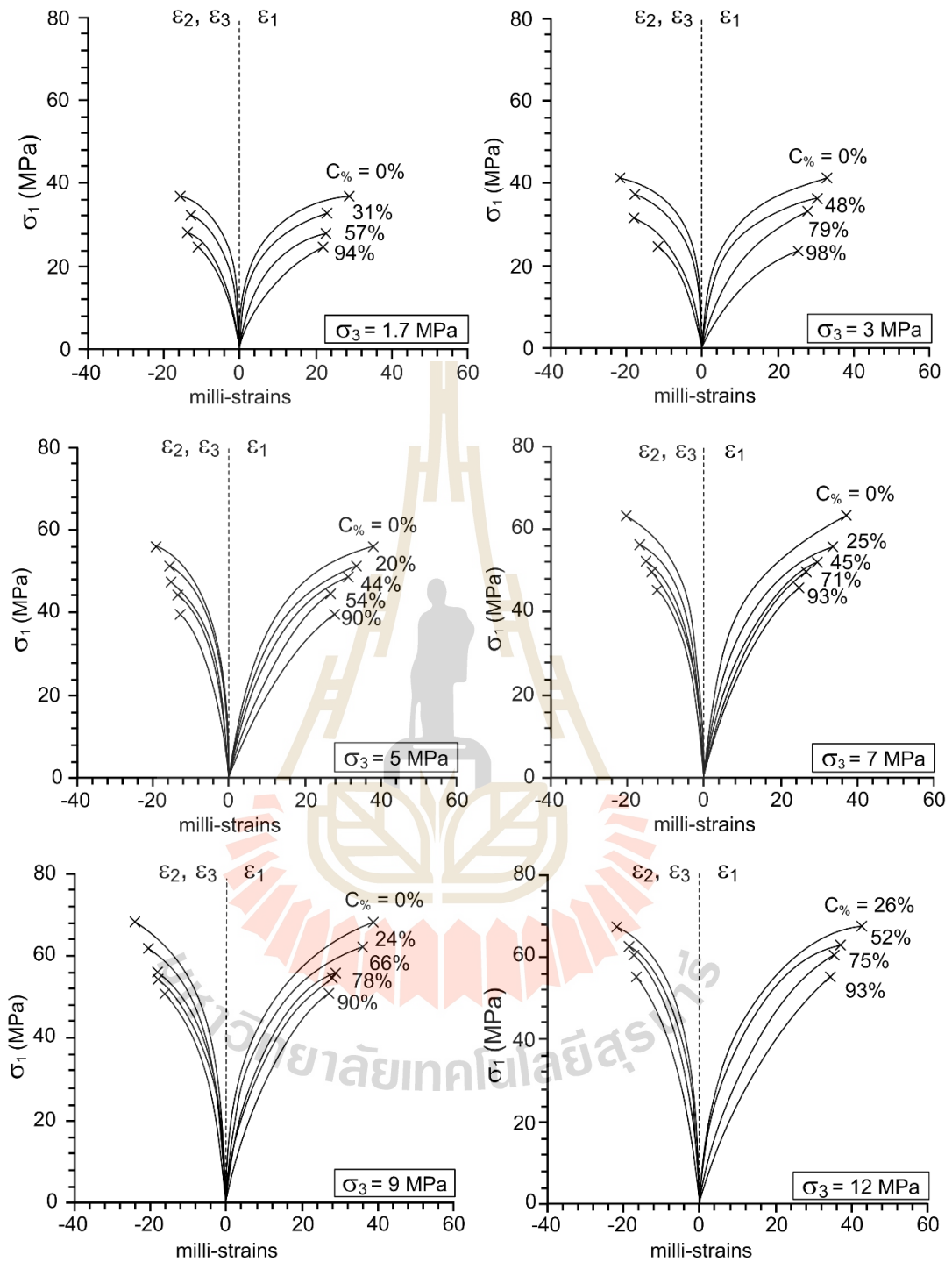


Figure 4.8 Stress-strain curves obtained for triaxial strength testing.

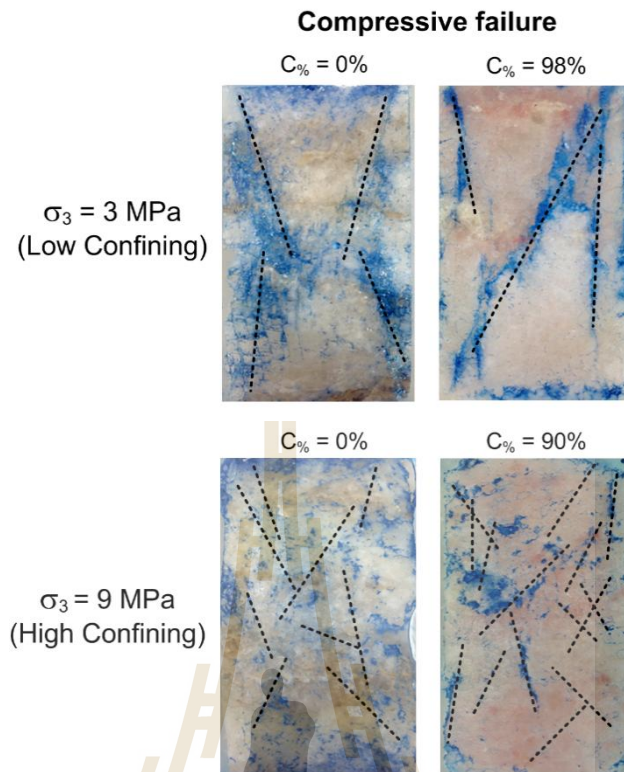


Figure 4.9 Some post-test specimens showing combination of shear failures.

4.6.5 Elastic parameter

The elastic modulus (E) and Poisson's ratio (ν) of the specimens can be determined by assuming that the specimens are isotropic, and hence the shear (rigidity) modulus (G), Lamé' constant (λ), and Poisson's ratio (ν) can be calculated from (Jaeger et al., 2007):

$$G = (1/2) (\tau_{\text{oct}} / \gamma_{\text{oct}}) \quad (4.6)$$

$$3\sigma_m = (3\lambda + 2G) \varepsilon_v \quad (4.7)$$

$$\nu = \lambda / (2(\lambda + G)) \quad (4.8)$$

$$E = (2 (1 + \nu)) G \quad (4.9)$$

where τ_{oct} , γ_{oct} , σ_m and ε_v are the octahedral shear stress and strain, mean stress, and volumetric strain at dilation (the point where the elastic parameters are determined).

The elastic modulus rapidly decreases with increasing $C_{\%}$ (Figure 4.10(a)):

$$E = 16.81 \cdot \exp(-0.021 \cdot C_{\%}) \quad \text{GPa} \quad (4.10)$$

Extrapolation of the above equation suggests that pure carnallite specimens would have the elastic modulus of less than 2 GPa. The increase of the Poisson's ratio with increasing carnallite contents can be represented by a linear equation (Figure 4.10(b)):

$$\nu = 0.002 \cdot C_{\%} + 0.26 \quad (4.11)$$

Table 4.1 summarizes the strengths and elastic parameters obtained from triaxial testing. The results suggest that under loading the carnallite tends to dilate more than testing. The results suggest that under loading the carnallite tends to dilate more than halite. This is probably due to the fact that carnallite is softer and has no cleavage while the stronger halite crystal has three mutually perpendicular cleavage planes.

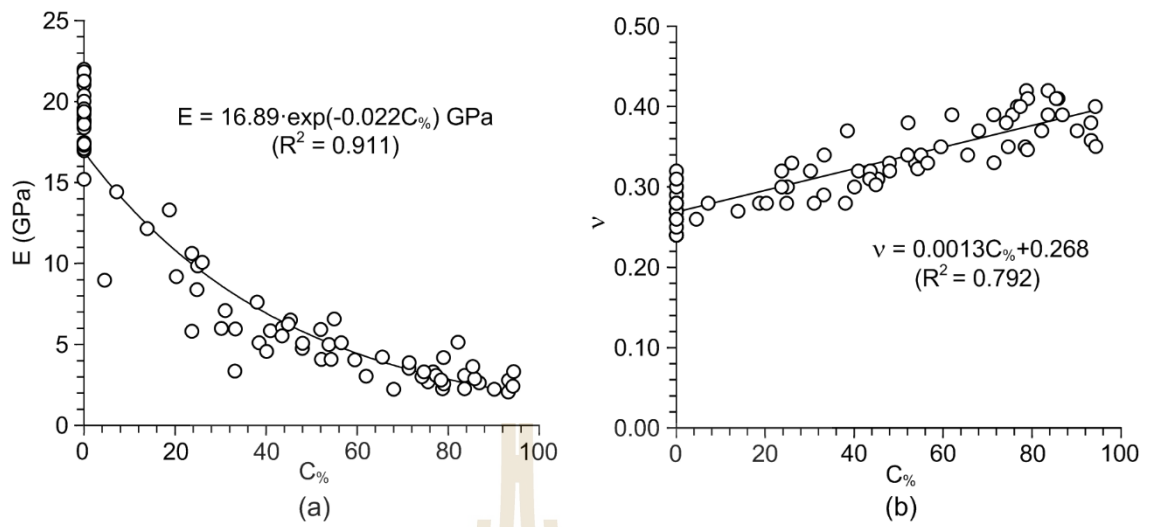


Figure 4.10 Elastic modulus (a) and Poisson's ratio (b) as function of carnallite content.

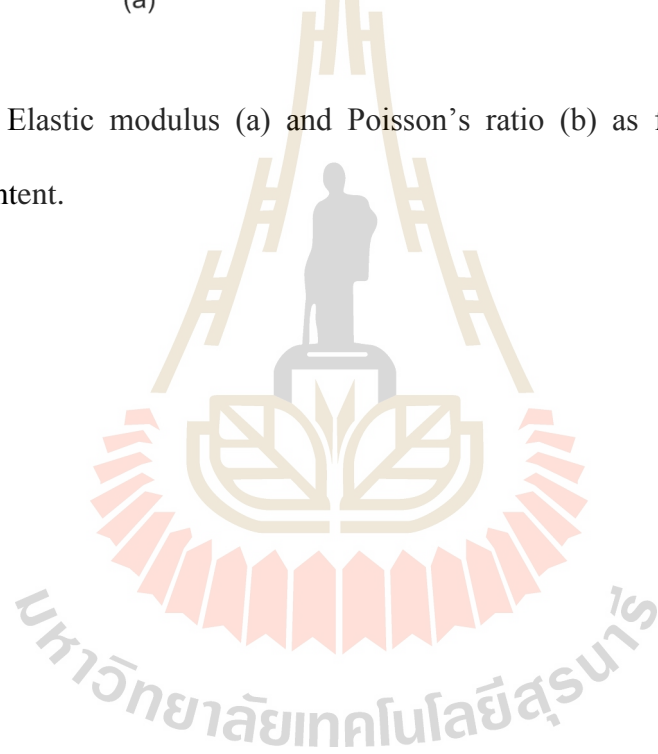


Table 4.1 Summary of the strength results and Elastic parameters obtained from triaxial compression tests.

σ_3 (MPa)	C%	$\sigma_{1,d}$ (MPa)	$\sigma_{1,f}$ (MPa)	G (GPa)	λ (GPa)	ν	E (GPa)
0	96	1.09	7.3	0.7	6.7	0.45	2.1
	95	1.21	7.4	0.8	7.1	0.45	2.3
	94	1.09	7.5	0.7	6.1	0.45	2.1
	92	1.29	7.7	0.8	6.7	0.44	2.4
	91	1.32	7.8	0.9	6.6	0.44	2.5
	90	1.34	7.9	0.9	6.5	0.44	2.5
	84	1.52	8.5	1.0	6.0	0.43	2.9
	81	1.62	8.8	1.1	5.8	0.42	3.1
	78	1.73	9.1	1.2	5.7	0.42	3.3
	77	1.76	9.2	1.2	5.7	0.41	3.3
	75	1.84	9.4	1.2	5.6	0.41	3.5
	73	1.92	9.7	1.3	5.6	0.41	3.6
	70	2.04	10.0	1.4	5.5	0.40	3.9
	69	2.09	10.1	1.4	5.5	0.40	3.9
	68	2.13	10.3	1.4	5.5	0.40	4.0
	65	2.27	10.6	1.5	5.5	0.39	4.3
	62	2.42	11.0	1.7	5.5	0.38	4.6
	61	2.47	11.2	1.7	5.5	0.38	4.7
	60	2.52	11.3	1.7	5.5	0.38	4.8
	57	2.69	11.7	1.8	5.5	0.37	5.1
55	2.80	12.0	1.9	5.5	0.38	5.3	
54	2.86	12.1	2.0	5.5	0.37	5.4	
53	2.92	12.3	2.0	5.5	0.37	5.5	

Table 4.1 Summary of the strength results and Elastic parameters obtained from triaxial

σ_3 (MPa)	C%	$\sigma_{1,d}$ (MPa)	$\sigma_{1,f}$ (MPa)	G (GPa)	λ (GPa)	ν	E (GPa)
0	51	3.05	12.6	2.1	5.5	0.36	5.8
	50	3.11	12.7	2.2	5.6	0.36	5.9
	46	3.38	13.4	2.4	5.6	0.35	6.4
	45	3.46	13.5	2.4	5.6	0.35	6.5
	44	3.53	13.7	2.5	5.7	0.35	6.7
	37	4.09	14.9	2.9	5.8	0.33	7.7
	24	5.37	17.4	3.9	6.2	0.31	10.2
	19	5.97	18.5	4.3	6.4	0.30	11.3
	14	6.63	19.6	4.9	6.6	0.29	12.5
	14	6.63	19.6	4.9	6.6	0.29	12.5
	13	6.77	19.8	5.0	6.6	0.29	12.8
	11	7.06	20.3	5.2	6.7	0.28	13.3
	11	7.06	20.3	5.2	6.7	0.28	13.3
	9	7.36	20.8	5.4	6.8	0.27	13.9
	9	7.36	20.8	5.4	6.8	0.28	13.9
	9	7.36	20.8	5.4	6.8	0.29	13.9
	7	7.67	21.3	5.7	6.9	0.28	14.5
	5	8.00	21.8	6.0	7.0	0.27	15.1
	5	8.00	21.8	6.0	7.0	0.25	15.1
	4	9.17	22.7	6.1	7.0	0.27	15.3
4	8.14	22.1	6.2	7.6	0.26	15.5	
4	9.57	23.1	6.4	7.0	0.27	15.7	
0	8.89	24.2	6.7	7.2	0.26	16.8	

	0	8.56	21.2	6.7	7.5	0.26	17.0
--	---	------	------	-----	-----	------	------

compression tests (cont.).

σ_3 (MPa)	C%	$\sigma_{1,d}$ (MPa)	$\sigma_{1,f}$ (MPa)	G (GPa)	λ (GPa)	ν	E (GPa)
---------------------	----	-------------------------	-------------------------	------------	--------------------	-------	------------



Table 4.1 Summary of the strength results and Elastic parameters obtained from triaxial

0	0	8.84	23.2	6.7	7.6	0.25	16.2
	0	8.89	27.9	6.9	7.7	0.26	18.7
	0	8.51	25.2	7.0	7.9	0.27	16.6
	0	8.86	23.4	6.7	7.6	0.26	17.3
1.7	94	6.7	25	1.3	1.0	0.35	3.3
	57	8.9	28.1	2.0	1.8	0.33	5.1
	31	12.4	32.5	2.8	2.4	0.29	9.9
	0	18.5	37.6	8.2	6.0	0.27	20
3	79	12.3	32.8	1.6	1.6	0.34	4.4
	48	15.4	36.9	1.8	5.2	0.32	6.1
	0	24.7	45.1	7.0	6.4	0.26	15.8
	0	26.3	41.9	7.7	7.8	0.27	16.6
5	94	13.0	39.7	0.9	1.6	0.4	2.4
	54	17.7	45.1	2.0	1.9	0.33	5.7
	44	22.3	47.4	2.1	3.4	0.31	8.6
	20	25.0	51.9	3.6	4.1	0.3	10.5
	0	32.4	54.1	9.5	11.3	0.27	16.9
	0	32.1	56	8.0	14.9	0.27	17.1
7	93	16.8	46	0.8	1.9	0.38	3.0
	71	19.4	50.4	1.4	2.7	0.35	4.2
	45	24.3	52.7	2.4	3.4	0.31	7.0
	25	28.	56.1	3.9	6.1	0.28	9.9
	0	37.7	63.6	10.1	13.8	0.26	16.1
	0	38.4	60	7.01	15.3	0.26	16.5

compression tests (cont.).

Table 4.1 Summary of the strength results and Elastic parameters obtained from triaxial

compression tests (cont.).

σ_3 (MPa)	C%	$\sigma_{1,d}$ (MPa)	$\sigma_{1,f}$ (MPa)	G (GPa)	λ (GPa)	ν	E (GPa)
9	90	18.9	50.2	0.8	2.1	0.4	2.9
	78	21.8	53	1.0	2.3	0.37	4.2
	66	24.5	54.7	1.5	3.0	0.35	5.3
	24	31.9	60.8	3.9	9.0	0.29	10.2
	0	42.6	67	7.4	14.57	0.27	16.1
12	93	23.9	55.8	0.7	2.6	0.4	3.5
	75	27.9	61.4	1.2	2.9	0.38	4.8
	52	35.1	63.6	2.4	4.9	0.34	7.7
	26	41.0	68.1	4.1	7.2	0.3	10.8
	0	41.0	71.1	6.6	15.4	0.26	16.3
	0	51.0	81.2	10.9	4.5	0.26	16.9

CHAPTER V

STRENGTH CRITERIA

5.1 Introduction

The strength criteria used in this study include the Hoek and Brown, Yudhbir, empirical equation and strain energy density criteria. The principal stresses at failure are used to calibrate the strength parameters. The coefficient of correlation is calculated for each criterion to determine its predictive capability. These calibrated criteria will be used to predict the extraction ratio and stability condition of circular hole in infinite medium which will be presented in chapter VI and VII

5.2 Strength criteria

Hoek and Brown strength criterion

The Hoek-Brown strength criterion (Hoek and Brown, 1980) is used here to describe the relationship between the major (σ_1) and minor (σ_3) principal stresses at dilation and at failure of the triaxial test results:

$$\sigma_1 = \sigma_3 + (m \cdot \sigma_3 \cdot \sigma_c + s \sigma_c^2)^{1/2} \quad (5.1)$$

where m and s are material constants. For intact specimens used in this study, $s = 1$. The criterion can be rewritten as function of principal stresses at dilation and at failure:

$$\sigma_{1,d} = \sigma_3 + (m_d \cdot \sigma_3 \cdot \sigma_{c,d} + s\sigma_{c,d}^2)^{1/2} \quad (5.2)$$

$$\sigma_{1,f} = \sigma_3 + (m_f \cdot \sigma_3 \cdot \sigma_{c,f} + s\sigma_{c,f}^2)^{1/2} \quad (5.3)$$

where m_d and m_f represent the conditions at dilation and at failure. Via regression analysis they can be defined as a function of $C\%$ as:

$$m_d = -0.085 \cdot C\% + 14.73 \quad (5.4)$$

$$m_f = -0.033 \cdot C\% + 18.09 \quad (5.5)$$

By substituting Equations (4.2), (4.3), (5.4) and (5.5) into Equations (5.2) and (5.3), the complete dilation and failure criteria for specimens with varied $C\%$ can be obtained. Figure 5.1 compares the criteria with the strength data. Good correlation is obtained ($R^2 > 0.9$). The results suggest that the specimens become softer as the $C\%$ increases, as evidenced by the decrease of parameter m (Figure 5.2).

Yudhbircriterion

Yudhbir et al. (1983) modify the original Bieniawski criterion (1974). The new criterion can be written in a more general form as:

$$\sigma_{1,d}/\sigma_c = A + B(\sigma_3/\sigma_{c,d})^b \quad (5.6)$$

$$\sigma_{1,f}/\sigma_c = A + B(\sigma_3/\sigma_{c,f})^b \quad (5.7)$$

where A is b dimensionless parameter whose value depends on rock mass quality, and B is material constant depending on rock type. Figure 5.3 compare the criterion with the test results in the terms of σ_1 as a function of σ_3 at dilation and at failure.

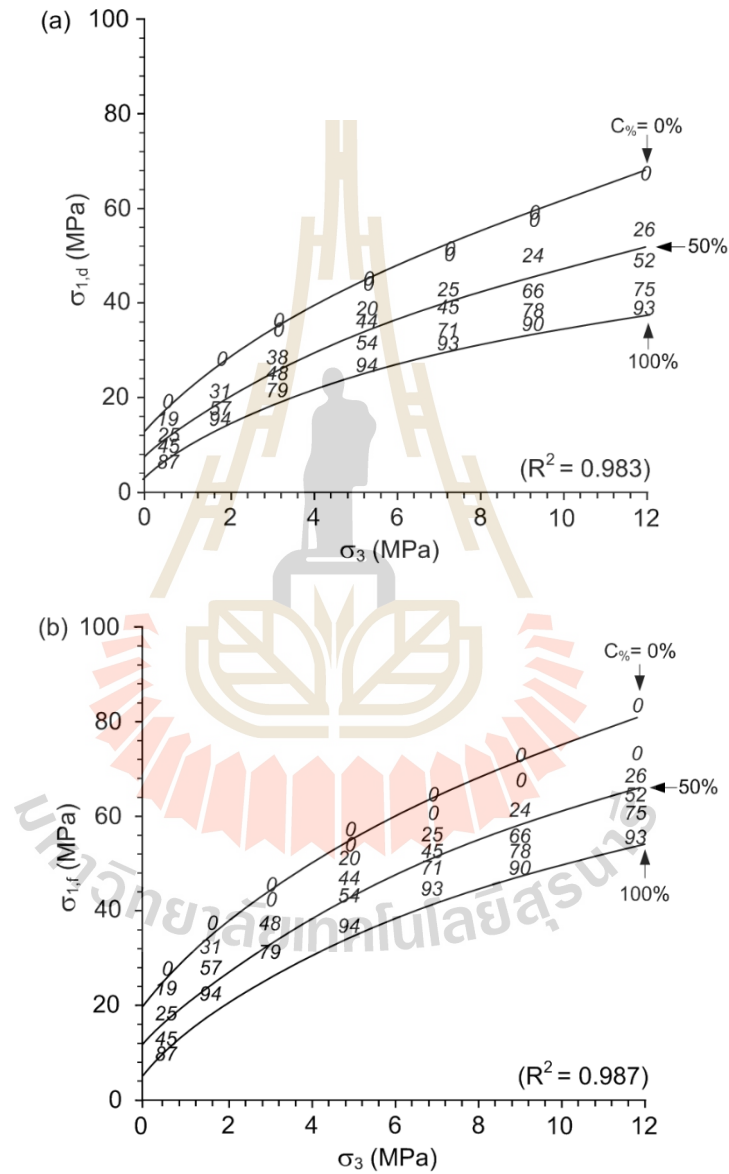


Figure 5.1 Major principal stresses at dilation (a) and at failure (b) as a function of minor principal stress. Hoek-Brown strength criterion fitted to strength data. Numbers in the diagrams indicate carnallite contents.

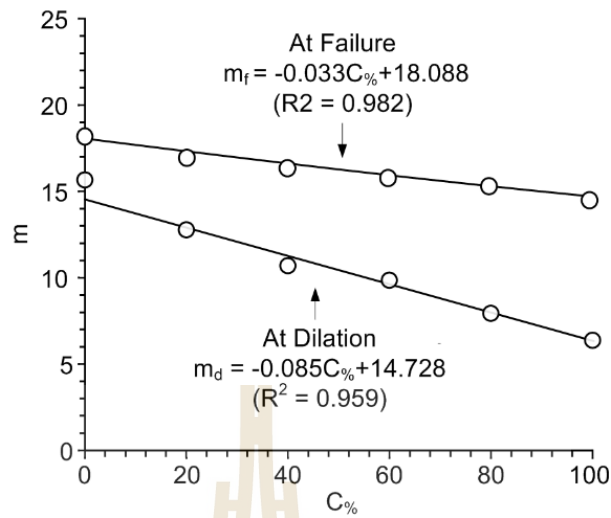


Figure 5.2 Hoek-Brown parameter m as a function of carnallite content.

Empirical equation

An empirical equation is proposed to predict the compressive strengths under various confining pressures and carnallite contents:

$$\sigma_{1,d} = C + D \sigma_3^d \quad (5.8)$$

$$\sigma_{1,f} = C + D \sigma_3^d \quad (5.9)$$

where σ_c is the salt compressive strength (MPa), C , D and d are empirical constants.

Figure 5.4 compares the test data with curve fits of the strength criterion in the terms of σ_1 as a function of σ_3 at dilation and at failure. Good correlation is obtained for both dilation and failure conditions.

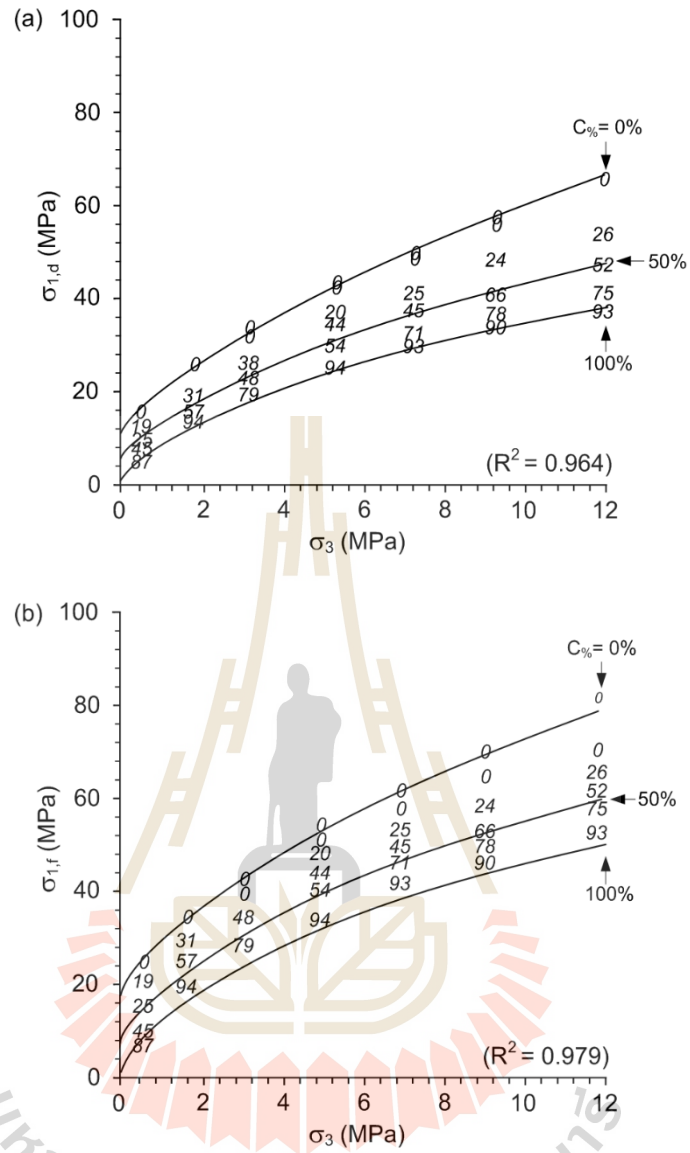


Figure 5.3 Major principal stresses at dilation (a) and at failure (b) as a function of minor principal stress. Yudhbircriterion fitted to strength data. Numbers in the diagrams indicate carnallite contents.

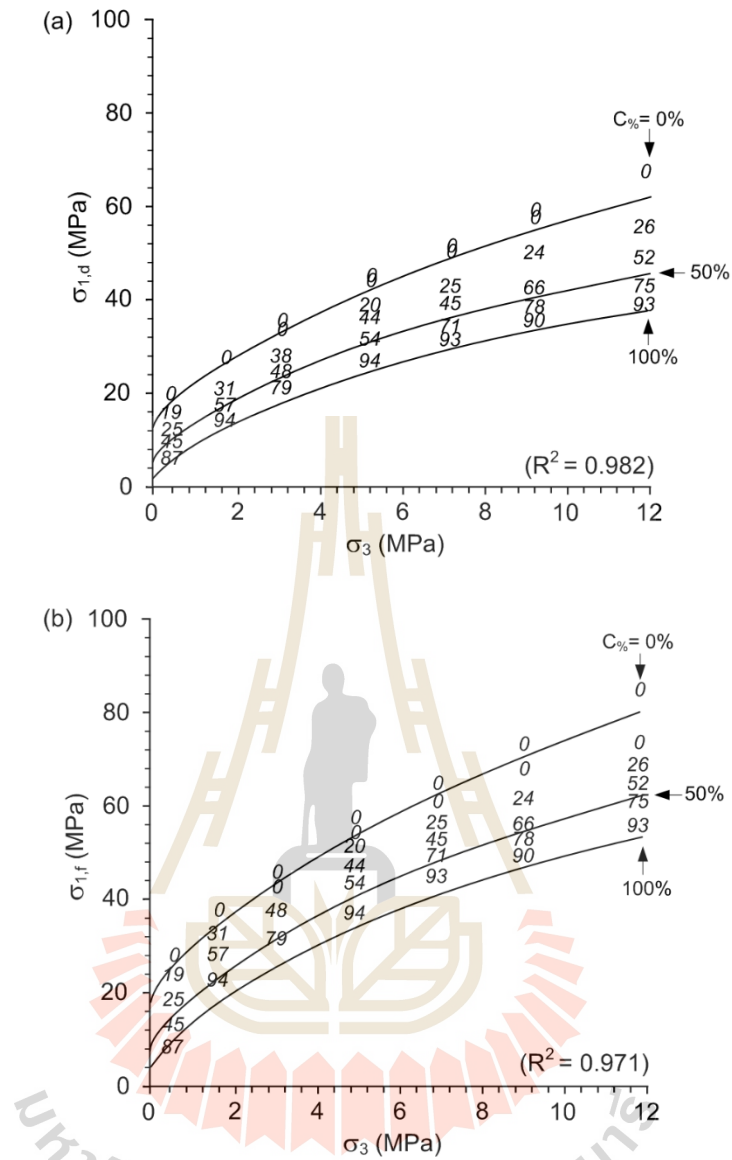


Figure 5.4 Major principal stresses at dilation (a) and at failure (b) as a function of minor principal stress. Empirical equation fitted to strength data. Numbers in the diagrams indicate carnallite contents.

5.3 Strength criterion based on strain energy principle

The strain energy density principle is applied here to describe the rock strength and deformation under different confining pressure. The distortional strain energy at dilation ($W_{d,d}$) and at failure ($W_{d,f}$) can be calculated from the shear modulus and octahedral shear stresses for each rock specimen as follows (Jaeger et al., 2007):

$$W_d = (3/2) \cdot \tau_{oct,f} \cdot \gamma_{oct,f} \quad (5.10)$$

$$W_{d,d} = (3/2) \cdot \tau_{oct,d} \cdot \gamma_{oct,d} \quad (5.11)$$

where $\tau_{oct,f}$, $\tau_{oct,d}$ are octahedral shear stress at failure and at dilation, $\gamma_{oct,f}$, $\gamma_{oct,d}$ are octahedral shear strain at failure and at dilation.

It is assumed that under a given mean stress the distortional strain energy required to dilate and to fail the rock salt specimens is constant. The distortional strain energy linearly increases with the mean stress:

$$W_{d,d} = \{ [(-\varpi \cdot C\%) + \varpi'] \cdot \sigma_m + ((-\xi \cdot C\%) + \xi') \} \quad \text{MPa} \quad (5.12)$$

$$W_{d,f} = \{ [(-\omega \cdot C\%) + \omega'] \cdot \sigma_m + ((-\zeta \cdot C\%) + \zeta') \} \quad \text{MPa} \quad (5.13)$$

where ϖ , ϖ' , ξ , ξ' , ω , ω' , ζ and ζ' are empirical constants. For the MahaSarakhm salt they are defined as: 0.00011, 0.027, 0.0001, 0.031, 0.00015, 0.038, 0.0004 and 0.055, respectively. Equations (5.12) and (5.13) can be used to predict the rock salt strength and dilation in terms of the maximum distortional strain energy that salt can absorb before dilation or failure occurs. Figure 5.5 compares the strength criteria with the

strength data. Vary good correlation coefficients are obtained both at dilation and failure.

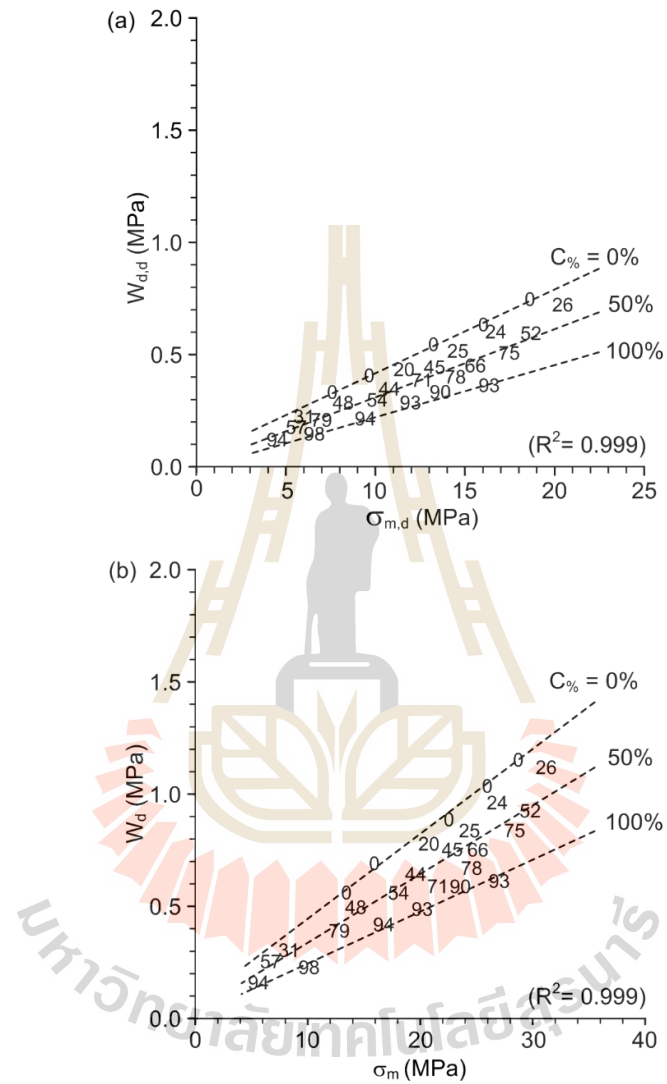


Figure 5.5 Distortional strain energy at dilation ($W_{d,d}$) and at failure ($W_{d,f}$) as a function of mean stress (σ_m) for various confining pressures (σ_3) and carnallite content ($C\%$).

CHAPTER VI

PILLAR STABILITY

6.1 Introduction

The objective of this chapter is to determine the stability of pillars and extraction ratios of potash mines. The strength criteria developed by Hoek and Brown, Yudhbir, empirical equation and strain energy density principle given in the previous chapter will be applied in the analysis.

6.2 Extraction ratio

The tributary area concept is first applied here to determine the extraction ratio of mine horizon at different depths (100 m-400 m). To describe the extraction ratio in terms of pillar stress, the expression obtained by Biron and Arioglu (1980) can be used :

$$e = 1 - [(\gamma \cdot H) / \sigma_p] \times 100 \quad (6.1)$$

where e is the extraction ratio, H is depth of cover, γ is average rock unit weight, and σ_p is the pillar stress.

The pillar stress can be calculated from the compressive strength of the rock with appropriate factor of safety (FS.)

$$\sigma_p = \sigma_c / FS.$$

(6.2)



where (σ_c) represents the uniaxial compressive strength at dilation and at failure under various carnallite contents. Figures 6.1 and 6.2 compare the extraction ratios as a function of carnallite content at dilation and at failure. Extraction ratio depends on the strength of the rock salt, depth and factor of safety. The ratios at dilation and at failure decrease with increasing $C_{\%}$ and depth. Figure 6.1(a) shows extraction ratio calculated by Hoek and Brown criteria (Equations 5.2 and 5.3). Figure 6.1(b) shows the Yudhbir criterion (Equations 5.10 and 5.11). The result indicates that the extraction ratio at failure is greater than at dilation. The extraction ratios from empirical equation shown in Figure 6.2(a) and in Figure 6.2(b) are obtained by the strain energy density criterion. They are lower than those obtained from other strength criteria. This is because the strain energy density considers both stress and strain at failure, and hence their results would be more comprehensive than the others.

Based on the chemical compositions the carnallite contains 26.8% by weight of sylvite (KCl) which is of interest here (Klein et al., 1988). At 100, 200, 300 and 400 m depths, and for the factor of safety of 1.1 the amount of KCl can be related to the extraction ratio as:

$$KCl = [(26.8 \cdot C_{\%}) / 100] \times e \quad (6.3)$$

Figures 6.3 and 6.4 show the weight percent of sylvite (KCl) as a function of $C_{\%}$ for various depths under $F.S = 1.1$ at 100, 200, 300 and 400 m depths. Figure 6.3 shows the weight percent of sylvite (KCl) calculated by the Hoek and Brown criterion and Yudhbir criterion. Figure 6.4 shows weight percent of sylvite (KCl) calculated by empirical equation and by strain energy density criterion. The amount of KCl that can

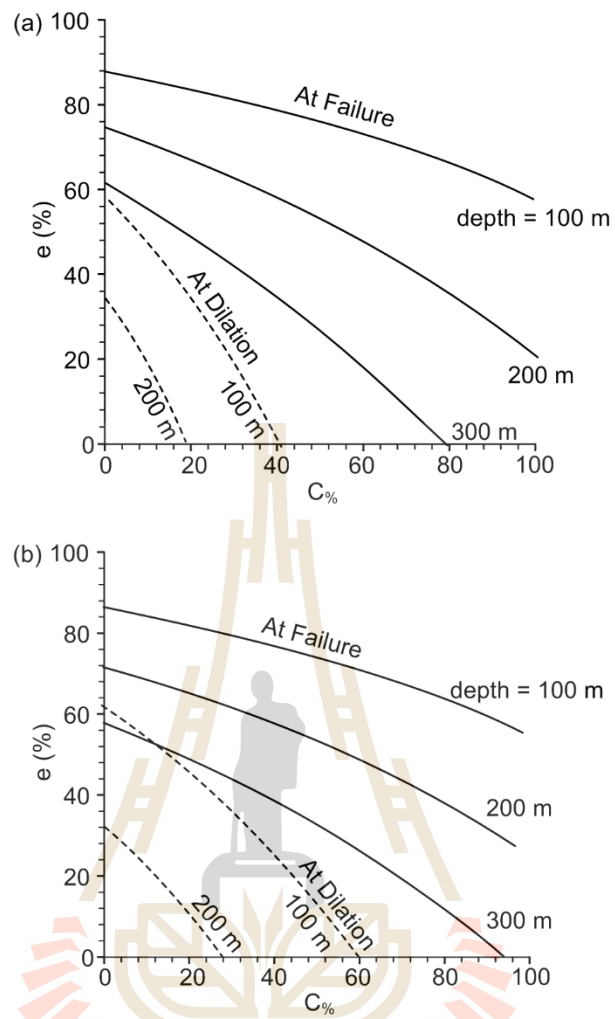


Figure 6.1 Extraction ratio as a function of carnallite content ($C_{\%}$) from Hoek and

Brown criterion (a) and Yudhbir criterion (b) for various depths.

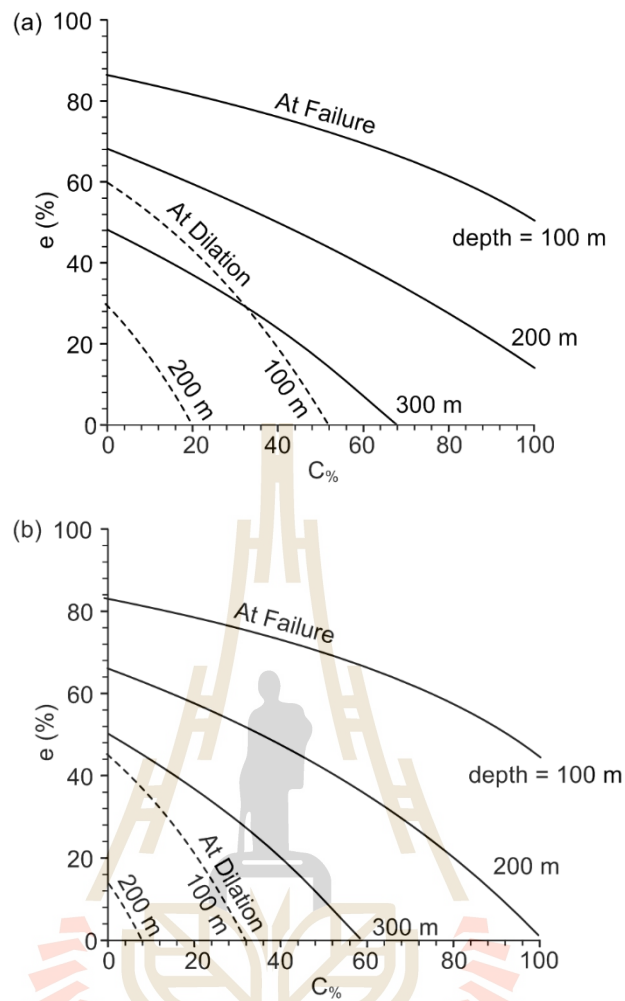
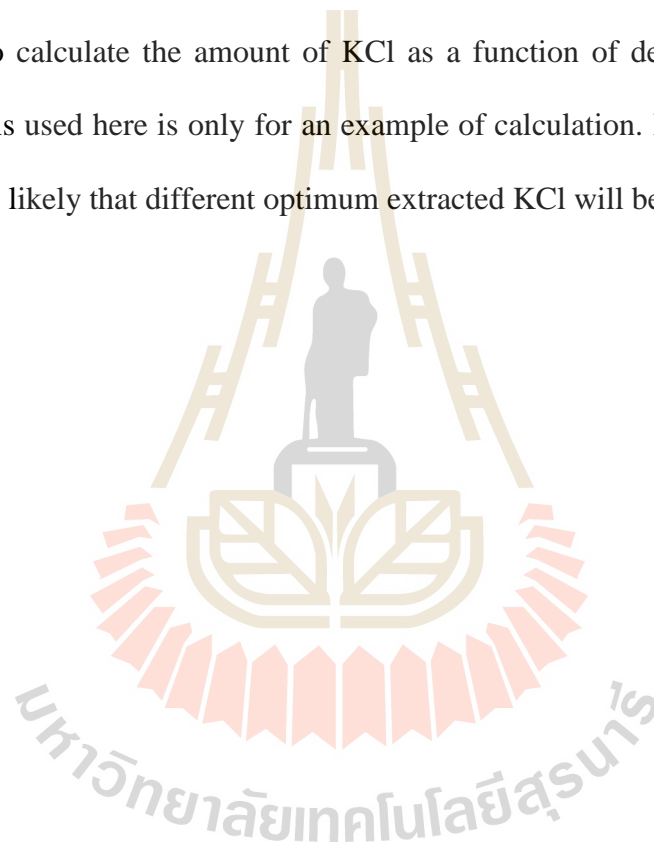


Figure 6.2 Extraction ratio as a function of carnallite content ($C\%$) from empirical equation(a) and strain energy density criteria (b) for various depths.

be extracted initially increases with $C\%$ until an optimum value is reached. Then the extracted KCl decreases under large amount of $C\%$. The lower depths show lower extracted KCl. The extracted KCl is greatest when Yudhbir criterion is used, and is lowest when the strain energy principle is applied. The diagrams in Figures 6.3 and 6.4 can be used to make an initial plan for the potash mines while considering the amount of carnallite, depth and factor of safety. Note that different FS. values can also be applied to calculate the amount of KCl as a function of depth and $C\%$. The FS. value of 1.1 is used here is only for an example of calculation. If different FS. values are used, it is likely that different optimum extracted KCl will be obtained.



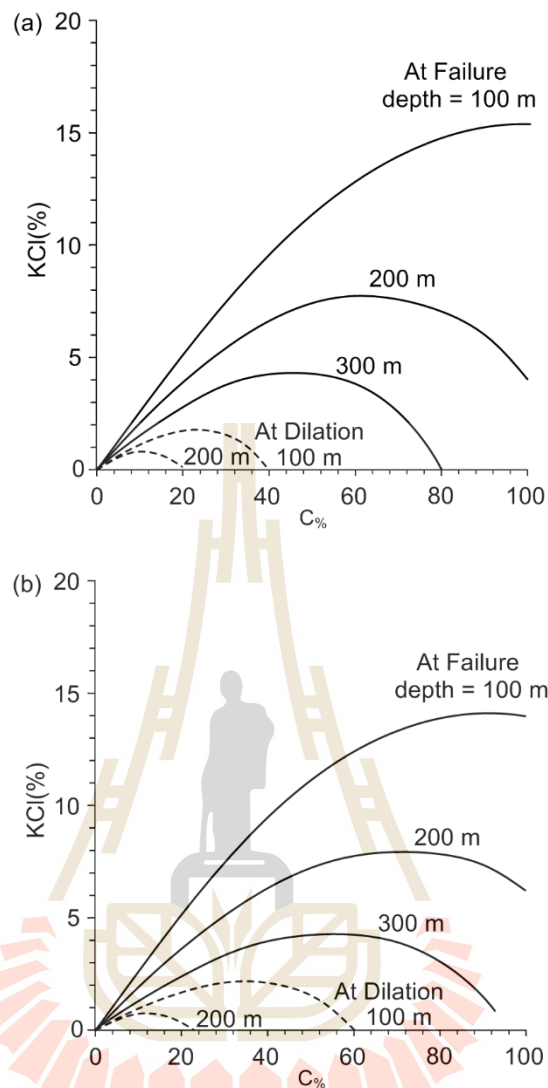


Figure 6.3 Weigh percent of sylvite (KCl) as a function of $C\%$ from Hoek and Brown criterion (a) and Yudhbir criterion(b) for various depths.

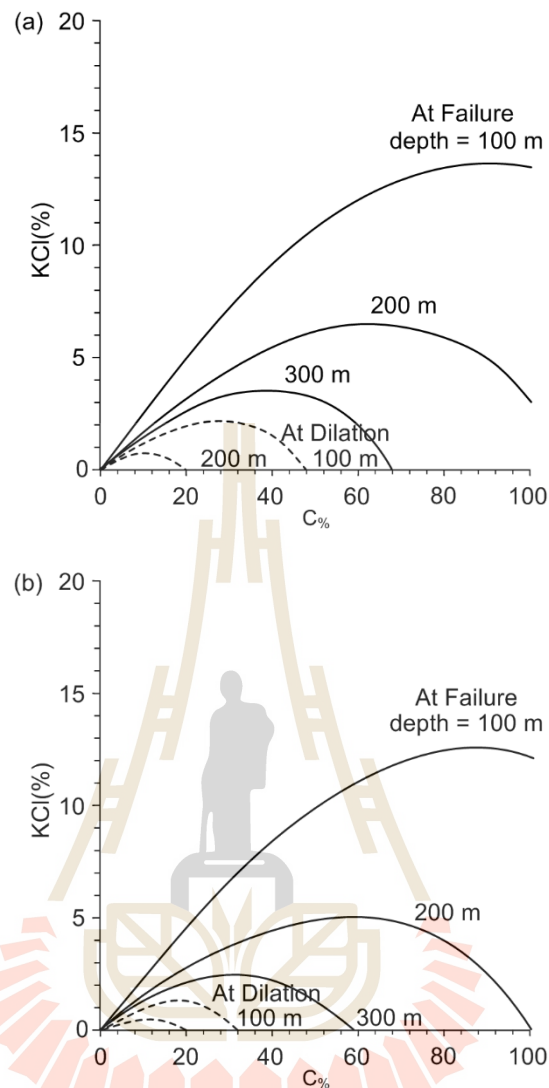


Figure 6.4 Weigh percent of sylvite (KCl) as a function of $C\%$ from empirical equation (a) and strain energy criterion (b) for various depths.

CHAPTER VII

SHAFT STABILITY

7.1 Introduction

The objective of this chapter is to determine stability of shaft in potash mines. The Hoek and Brown, Yudhbir, empirical equation and strain energy density criteria derived as a function of $C_{\%}$ are used to determine the extents of dilation and failure zones in rock salt around circular opening.

7.2 Shaft stability

To investigate the stability of shaft that penetrates rock salt with varied carnallite contents, the Kirsch's solution is adopted here to determine the stress distribution around circular hole in infinite plate subjected to uniform external pressures without internal pressure. The radial ($\sigma_r(r)$) and tangential ($\sigma_{\theta}(r)$) stresses can be calculated by (Jaeger et al., 2007):

$$\sigma_r(r) = \left[1 - \left(\frac{a^2}{r^2} \right) \right] \cdot P_o \quad (7.1)$$

$$\sigma_{\theta}(r) = \left[1 + \left(\frac{a^2}{r^2} \right) \right] \cdot P_o \quad (7.2)$$

where P_o is external pressure, a is hole radius and r is radial distance from the center. Under plane strain condition the axial stress is defined as: $\sigma_z(r) = \nu (\sigma_r(r) + \sigma_\theta(r))$. The calculated tangential and radial stresses for $r \geq a$ are compared against the strength criteria (chapter V) to determine the extents of the dilation and failure zones. The factors of safety are calculated for the depths of 100, 200, 300 and 400 m which are equivalent to P_o of 2.7, 5.4, 8.1 and 10.8 MPa.

The factors of safety at dilation and failure are defined as:

$$FS. = \sigma_{1,d}(r)/\sigma_\theta(r) \quad (7.3)$$

$$FS. = \sigma_{1,f}(r)/\sigma_\theta(r) \quad (7.4)$$

where $\sigma_{1,d}$ is major principal stress at dilation and $\sigma_{1,f}$ is major principal stress at failure. From the strength criteria in Chapter V $\sigma_{1,d}$ and $\sigma_{1,f}$ can be written as a function of major and minor principal stresses in terms of Kirsch's solution:

Hoek and Brown Criterion:
$$\sigma_{1,d}(r) = \sigma_r(r) + (m \cdot \sigma_r(r) \cdot \sigma_{c,d} + s \sigma_{c,d}^2)^{1/2} \quad (7.5)$$

$$\sigma_{1,f}(r) = \sigma_r(r) + (m \cdot \sigma_r(r) \cdot \sigma_{c,f} + s \sigma_{c,f}^2)^{1/2} \quad (7.6)$$

Yudhbir Criterion:
$$\sigma_{1,d}(r)/\sigma_c = A + B (\sigma_r(r) / \sigma_{c,d})^b \quad (7.7)$$

$$\sigma_{1,f}(r)/\sigma_c = A + B (\sigma_r(r) / \sigma_{c,f})^b \quad (7.8)$$

Empirical Equation:
$$\sigma_{1,d}(r) = C + D \sigma_r(r)^d \quad (7.9)$$

$$\sigma_{1,f}(r) = C + D\sigma_r(r)^d \quad (7.10)$$

where σ_c is compressive strength at dilation ($\sigma_{c,d}$) and at failure ($\sigma_{c,f}$). By substituting Equations (7.5), (7.7) and (7.9) into Equations (7.3) for the strength criteria at dilation. At failure substituting Equations (7.6), (7.8) and (7.10) into Equations (7.4). The zones of $FS \leq 1.0$ at dilation and failure around borehole can be presented as a function of r/a for various $C\%$ values in Figures 7.1 through 7.3, for $FS \leq 1.0$. The dilation and failure zones increase with carnallite contents and depths. The distortional strain energy at dilation and at failure is used to predict the stability zones along the borehole wall. The factors of safety at dilation and at failure are defined as:

$$FS = W_{d,d}(r)/W_d(r) \quad (7.11)$$

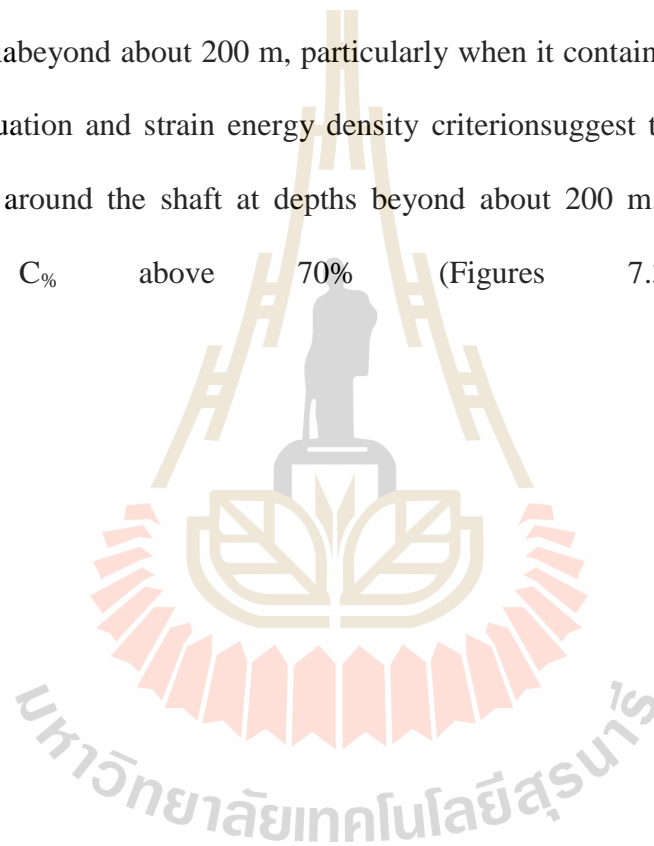
$$FS = W_{d,f}(r)/W_d(r) \quad (7.12)$$

The radial (u_r) and tangential (u_θ) displacements around the cylindrical hole under uniform stress field obtained from the elastic solution (Brady and Brown, 1985) can be expressed as:

$$u_r = -\frac{a^2}{4Gr} \left\{ P_o - P_o \left[2(1-2\nu) + \frac{a^2}{r^2} \right] \cos 2\theta \right\} \quad (7.13)$$

$$u_\theta = -\frac{a^2}{4Gr} \left\{ P_o \left[2(1-2\nu) + \frac{a^2}{r^2} \right] \sin 2\theta \right\} \quad (7.14)$$

The calculation results are shown in Figures 7.1 through 7.4. For the four criteria used in this study the extents of these zones increase with depth and $C_{\%}$. Yudhbir criterion gives the smallest dilation and failure zone while the strain energy density criterion gives the largest values. The diagrams suggest that rock salt around the shaft at depths beyond about 300 m for Yudhbir criterion may require artificial supports, particularly when it contains $C_{\%}$ above 50% (Figure 7.1) and for Hoek and Brown criteria beyond about 200 m, particularly when it contains $C_{\%}$ above 90%. The empirical equation and strain energy density criteria suggest that artificial supports are required around the shaft at depths beyond about 200 m, particularly when it contains $C_{\%}$ above 70% (Figures 7.3 and 7.4).



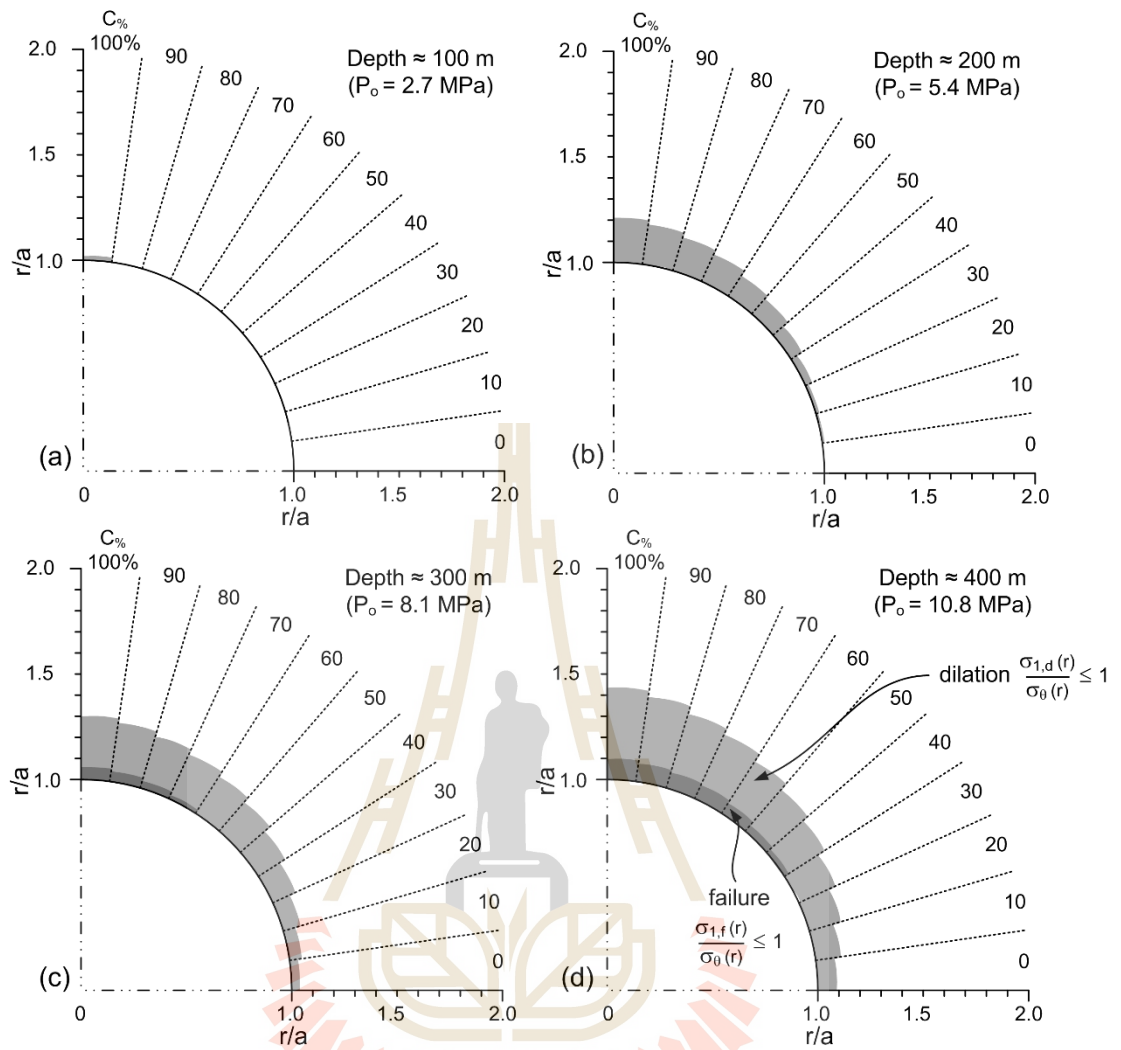


Figure 7.1 Dilation and failure zones induced in circular opening in rock salt under various carnallite contents for depths of 100 m (a), 200 m (b), 300 m (c), and 400 m (d) for Yudhbir criterion.

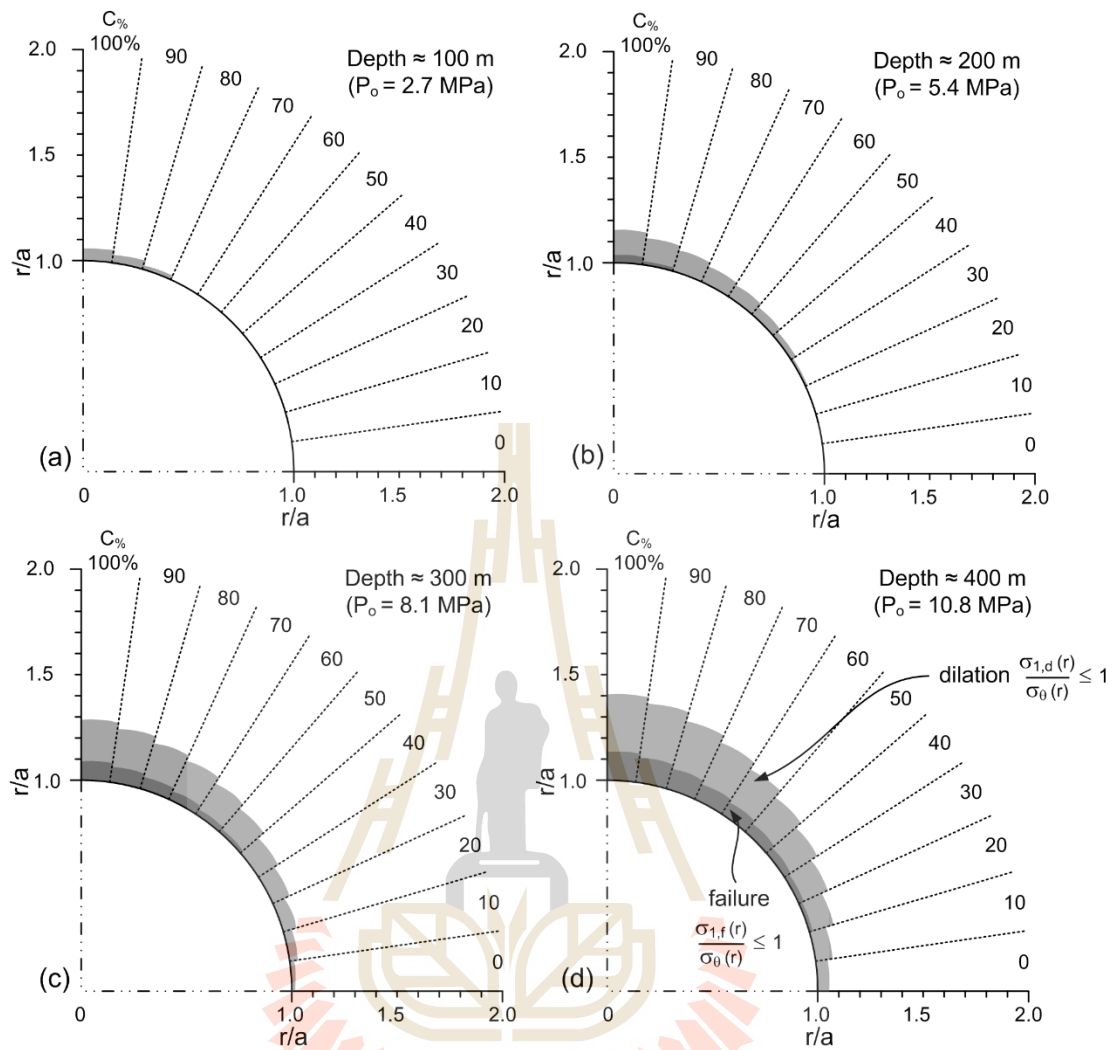


Figure 7.2 Dilation and failure zones induced in circular opening in rock salt under various carnallite contents for depths of 100 m (a), 200 m (b), 300 m (c), and 400 m (d) for Hoek and Brown criterion.

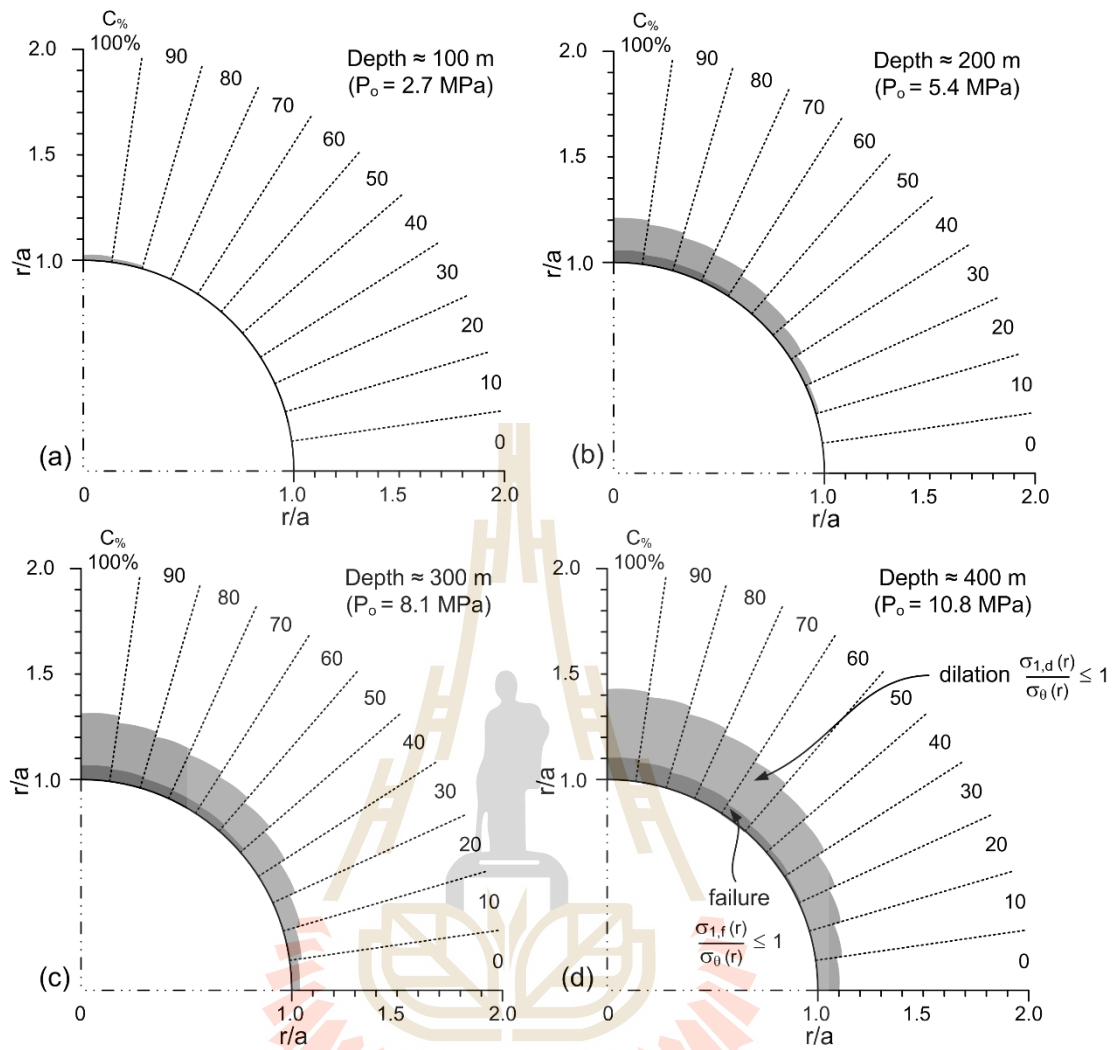


Figure 7.3 Dilation and failure zones induced in circular opening in rock salt under various carnallite contents for depths of 100 m (a), 200 m (b), 300 m (c), and 400 m (d) for empirical equation.

CHAPTER VIII

DISCUSSIONS, CONCLUSIONS AND RECOMMENDATIONS FOR FUTURE STUDIES

8.1 Discussions

This section discusses the key issues relevant to the reliability of the test schemes and the adequacies of the test results. Comparisons of the results and findings from this study with those obtained elsewhere under similar test conditions have also been made.

- The numbers of the test specimens seem adequate, as evidenced by the good coefficients of correlation for all confining pressure and carnallite content.
- The test results in terms of the stress-strain relations and strengths are believed to be reliable. They are agreed reasonably well with the related test results on the MahaSarakham salt obtained by Sriapai et al. (2012), (2013) and Sartkaew (2013).
- The proposed criteria are capable of describing the extents of dilation and failure zones in rock salt around circular opening. It is not intended here that the dilation associated criteria are better than the strength criteria. Depending on the site-specific requirements and local regulations, the factor of safety around circular opening may be defined by using other criteria.

- The strain energy density determined here is by assuming that the stress-strain relations are linear. In reality, however, non-linear behavior has been observed



for all test schemes and stress paths, in particular for the salt under large σ_3 and σ_m magnitudes. As a result the strain energy determined here is likely to underestimate the energy that the in-situ salt can absorb before dilation and failure. This makes the application of the strain energy criterion to the stability evaluation even more conservative.

- The advantage of the application of the strain energy density criterion over the strength criterion is that it considers both stress and strain at failure, and hence their results would be more comprehensive than the strength criteria.
- Calculation of the FS for the shaft clearly indicates that the stress distribution around the circular opening in salt mass is likely to increase with depth and carnallite content. This enhances the significance of the careful design of the shaft stability in potash mining.

8.2 Conclusions

(1) The effect of carnallite content can be observed from tensile strength and compressive strength decrease with increasing carnallite content, due to the fact that the orientations and amounts of halite and carnallite along the loading diameters and low strengths may be obtained for the tensile cracks that are largely induced through the carnallite crystals.

(2) The characterization results clearly show that the carnallite content can significantly reduce the strengths and elastic moduli of the rock salt. The tensile strength can reduce to less than 0.5 MPa when the $C_{\%}$ approaches 100%.

(3) The uniaxial compressive strengths of the pure carnallite is about 10 MPa

or less than half of those of the pure halite. The elastic modulus rapidly decreases from about 17GPa for pure halite to less than 2 GPa for pure carnallite specimens.

(4) The increases of the Poisson's ratio as the $C_{\%}$ increases is supported by the fact that the halite crystals contain cleavages and intergranular boundaries that can be compressed under loading. The carnallite crystals however have no cleavage and are relatively soft. As a results they are less compressible and tend to dilate more, as compared to the halite crystals.

(5) This study proposed strength criteriaincludethe Hoek and Brown, Yudhbir, empirical equation and strain energy density criterion. The four criteria can predict the salt strength under various carnallite content and confining pressure. The strain energy criterion is more conservative as it considers both stresses and strain at failure, which is similar to those of the actual condition occurred is soft rock, such as rock salt. Nevertheless, derivation of the strain energy criterion requires a more comprehensive measurements of the stress and strain at failure or at dilation during the laboratory testing.

(6) The strength criteria can represent the strengths of rock salt for the entire range of carnallite contents, both at dilation and at failure. The criterion indicates that the dilation and failure zones around circular hole increase with depth. These zones become significantly larger when the surrounding rock salt contains higher $C_{\%}$.

8.3 Recommendations for future studies

- Some uncertainties of the investigation and results discussed above lead to therecommendations for further studies. More testing is required on a variety of specimen with different of carnallite content. Determine contamination of

carnallite content by density may be inaccurate. Methods to determine the carnallite content inclusions should be developed for more precise determination. The test results under higher confining pressure should be obtained.

- Verification of the accuracy of the proposed criteria should be made by comparing with the actual salt opening (such as boreholes and shafts).



REFERENCES

- Artkhonghan, K. and Fuenkajorn, K. (2015). Effects of Stress Path on Polyaxial Strengths of MahaSarakham Salt. **Vietrock 2015 an ISRM Specialized Conference**. 12-13 March 2015, Hanoi, Vietnam.
- ASTM D3967-81. Standard test method for splitting tensile strength of intact rock core specimens. **Annual Book of ASTM Standards** (Vol. 04.08). Philadelphia: American Society for Testing and Materials.
- ASTM D5731-95. Standard test method for determination of the point load strength index of rock. **Annual Book of ASTM Standards** (Vol. 04.08). Philadelphia: American Society for Testing and Materials.
- ASTM D7012-07. Compressive strength and elastic moduli of intact rock core specimens under varying states of stress and temperatures. **Annual Book of ASTM Standards** (Vol. 04.08). Philadelphia: American Society for Testing and Materials.
- Bieniawski, Z.T. (1974). Estimating the strength of rock materials. **Journal of the South African Institute of Mining and Metallurgy**. 74: 312-320.
- Biron, E. and Arioglu. E. (1980). **Design of Supports in Mines**. A Wiley IntersciencePublication, Istanbul, Turkey. 270p.
- Boontongloan, C. (2000). Engineering properties of the evaporitic and clastic rocks of MahaSarakam Formation, SakonNakhonevaporite basin. **M.Sc. thesis**, School of Civil Engineering, Geotechnical Engineering, Asian Institute of Technology,

Thailand.

- Brady, B.H.G. and Brown, E.T. (1985). **Rock Mechanics for Underground Mining**, 3rd ed. George Allen and Unwin, Australia. 571p.
- Brown, E.T. (1981). Rock Characterization, Testing and Monitoring: **ISRM Suggested Methods, Published for the Commission on Testing Methods**, International Society for Rock Mechanics by Pergamon Press, Oxford, New York.
- Crosby, K.S. (2005). Overview of the geology and resources of the Udon Potash (sylvinite) deposits, UdonThani province, Thailand. In **Proceedings of International Conference on Geology, Geotechnology and Mineral Resources of Indochina** (pp.283-299), KhonKaen, Thailand.
- Devries, K.L., Mellegard, K.D., and Callahan, G.D. (2003). Laboratory testing in support of a bedded salt failure criterion. **SMRI: Fall 2003 meeting**. 5-8 October 2003, Chester, United Kingdom, England.
- Franssen, R.C.M.W. and Spiers, C.J. (1990). Deformation of polycrystalline salt in compression and in shear at 250-350 °C. In **Deformation Mechanism. Rheology and tectonics** (vol. 54(1), pp 201-213). Geological Society Special Publications.
- Fuenkajorn, K., Sriapai, T. and Samsri, P. (2012). Effects of loading rate on strength and deformability of MahaSarakham salt. **Engineering Geology**. 135: 10-23.
- Fuenkajorn, K., Walsri, C. and Phueakphum, D. (2011). Intrinsic variability of the mechanical properties of MahaSarakham salt. **Quarterly Journal of Engineering Geology and Hydrogeology**. 44: 445-456.

- Handin, J., Russell, J.E., and Carter, N.L. (1984). Transient Creep of Repository Rocks, Final Report: **Mechanistic Creep Laws for Rock Salts**, Texas A and M University, College Station, TX. 127p.
- Hansen, F.D., Mellegard, K.D., and Senseny, P.E. (1984). Elasticity and strength of ten natural rock salts. In **Proceeding of the 1st Conference on the Mechanical Behavior of Salt** (pp. 71-83). Clausthal Germany: Trans Tech Publications.
- Hawthorne, M. and Ferguson, J. (1976). **Physical Review**. B-13, APS Physics logo and Physics logo are trademarks of the American Physical Society. US.
- Hedley, D.G.F. (1967). An appraisal of convergence measurements in salt mines. In **Proceedings of the 4th Canadian Rock Mechanics Symposium** (pp. 117-135). Ottawa: Mines Branch, Dept of Mines and Technical Surveys.
- Hite, R.J. (1982). Progress Report on the Potash Deposits of the Khorat Plateau, Thailand, **Geological Survey, U.S.**
- Hite, R.J. and Japakasetr, T. (1979). Potash deposits of Khorat Plateau, Thailand and Laos. **Economic Geology**. 74 (2): 448-458.
- Hoek, E. and Brown, E.T. (1980). Empirical strength criterion for rock masses. **Journal of Geotechnical and Geoenvironmental Engineering**. 160(GT9): 1013-1035.
- Hoek, E., Carranza, C., and Corkum, B. (2002). Hoek-Brown failure criterion-2002 edition. In **Proceedings of the fifth North American rock mechanics symposium** (pp. 267-273), Toronto, Canada.

- Hurlbut, C.H. and Klein, C. (1977). **Manual of mineralogy**. 19th edition. Wiley. New York. 532p.
- Infante, E.F. and Chenevert, M.E. (1989). Stability of boreholes drilled through salt formations displaying plastic behavior. **International Journal of Rock Mechanics and Mining Sciences and Geomechanics Abstracts**. 26(6): 57-65.
- Jaeger, J.C., Cook, N.G.W., and Zimmerman, R.W. (2007). **Fundamentals of Rock Mechanics Fourth Edition**. Blackwell publishing, Oxford. 475p.
- Jandakaew, M. (2003). Experimental assessment of stress path effects on rock salt deformation. **M.Sc. thesis**, School of Geotechnology, Institute of Engineering, Suranaree University of Technology, Thailand.
- Klein, C., Hurlbut, C.S. and Dana, J.D. (1998). **Manual of Mineralogy**. John Wiley and Sons Inc. Wiley, New York. 571p
- Lux, K.H and Rokahr, R.B. (1984). Laboratory Investigations and Theoretical Statements as Basis for the Design of Caverns in Rock Salt Formations. In **Proceedings of the First Conference on the Mechanical Behaviour of Salt**. Penn State University, Trans Tech Publications.
- Mellegard, K.D., Robert, L.A. and Callahan, G.D. (2012). Effect of sylvite content on mechanical properties of potash. In **Proceedings of the Mechanical Behavior of Salt VII-Berest, Ghoreychi, Hadj-Hassen and Tijani** (pp. 71-79). Taylor and Francis Group, London.
- Morita, N. (2004). Well orientation effect on borehole stability. In **Proceedings SPE Annual Technical Conference and Exhibition**. (pp. 449-460). 26-29 September, Houston, Texas.

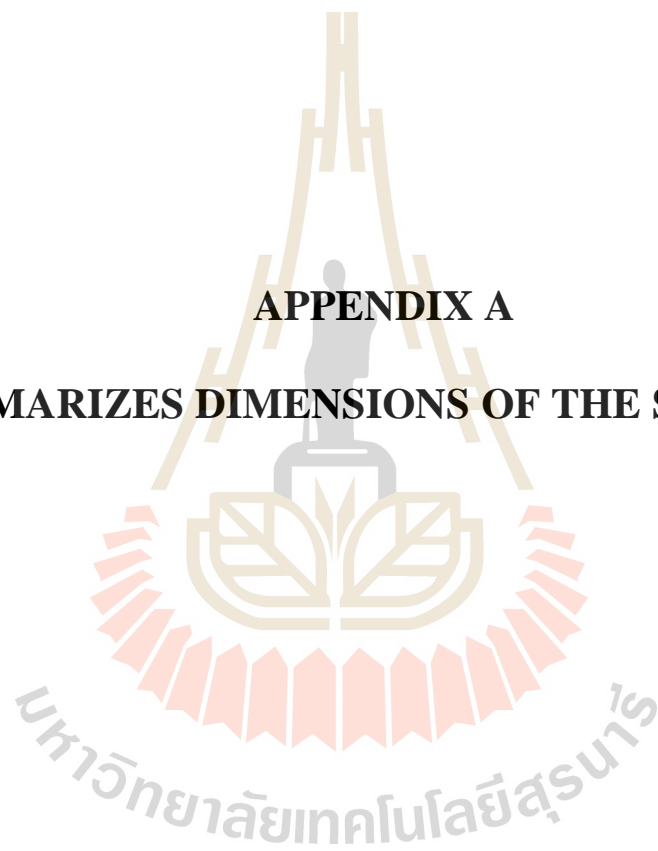
- Phueakphum, D. (2003). Compressed-air energy storage in rock salt of the MahaSarakham Formation. **M.Sc. thesis**, School of Geotechnology, Instituted of Engineering, Suranaree University of Technology, Thailand.
- Rafiai, H. (2011). New empirical polyaxial criterion for rock strength. **International Journal of Rock Mechanics and Mining Sciences**. 48: 922-931.
- Sartkeaw, S. and Fuenkajorn, K. (2013). Effect of stress rate on uniaxial compressive strength of rock salt under 0-100° C. **The 11th International Conference on Minerals and Petroleum Engineering** (pp.53-66). 11-13 November 2013, Chiang Mai, Thailand.
- Schlemper, E.O., Gupta, P.S.K., and Zoltai, T. (1985). Refinement of the structure of carnallite. **American Mineralogist**. 70: 1309-1313.
- Senseny, P.E., Hansen, F.D., Russell, J.E., Carter, N.L., and Handin, J.W. (1992). Mechanical behavior of rock salt: phenomenology and micromechanisms. **International Journal of Rock Mechanics and Mining Sciences**. 29(4): 363-378.
- Sriapai, T., Walsri, C., and Fuenkajorn, K. (2012). Effect of temperature on compressive and tensile strength of salt. **ScienceAsia**. 38: 166-174.
- Sriapai, T., Walsri, C., and Fuenkajorn, K. (2013). True-triaxial compressive strength of MahaSarakham salt. **International Journal of Rock Mechanics and Mining Sciences**. 61: 256-265.
- Suwanich, P. (1984). Potash and rock salt in Thailand. In **Conference on Geology and Mineral Resources of Thailand, Department of Mineral Resources** (pp. 244-252). Bangkok, Thailand.

- Suwanich, P. (2007). Potash-evaporite deposits in Thailand. In **Proceedings of the International Conference on Geology of Thailand** (pp. 252-262). 21-22 November 2007, Department of Mineral Resources, Thailand.
- Walsri, C., Poonprakon, P., Thosuwan R., and Fuenkajorn, K. (2009). Compressive and tensile strengths of sandstones under true triaxial stresses. In **Proceeding 2nd Thailand Symposium on Rock Mechanics** (pp 199- 218). Chonburi, Thailand.
- Weck, P.F., Kim, E., Carlos, F., Colon, J., and David, C.S. (2014). First-principles study of anhydrite, polyhalite and carnallite. **Chemical Physics Letters**. 594: 1-5.
- Wetchasat, K. (2002). Assessment of mechanical performance of rock salt formations for nuclear waste repository in northeastern Thailand. **M.S. thesis**, Suranaree University of Technology, Thailand.
- Wiebols, G.A. and Cook, N.G.W. (1968). An energy criterion for the strength of rock in polyaxial compression. **International Journal of Rock Mechanics and Mining Sciences**. 5: 529-549.
- Wisetsaen, S., Walsri, C., and Fuenkajorn, K. (2015). Effects of loading rate and temperature on tensile strength and deformation of rock salt. **International Journal of Rock Mechanics and Mining Sciences**. 73: 10-14.
- Yudhbir, L.W. and Prinzl, F. (1983). An empirical failure criterion for rock masses, In **Proceedings of the 5th International Congress Society of Rock Mechanics Melbourne**. 1: 1-8.

Zhou, S. (1994). A Program to Model the Initial Shape and Extent of Borehole Breakout. **Computers and Geosciences**. 20: 1143-1160.



APPENDIX A
SUMMARIZES DIMENSIONS OF THE SPECIMEN



TableA1 Specimen dimensions prepared for Brazilian tension test.

Specimen No.	Diameter (mm)	Length (mm)	Wight (mm)	Density (g/cc)	C%
BZ-01	63.1	30.3	193.3	2.05	20
BZ-02	60.0	29.5	180.9	2.17	0
BZ-03	62.5	28.1	170.2	1.97	33
BZ-04	61.5	29.4	170.3	1.95	37
BZ-05	63.6	30.8	182.1	1.86	53
BZ-06	62.8	31.4	187.1	1.92	42
BZ-07	62.9	30.3	157.6	1.67	87
BZ-08	62.8	30.5	159.8	1.68	85
BZ-09	62.9	30.5	163.5	1.72	78
BZ-10	62.8	30.5	185.2	1.96	35
BZ-11	61.4	30.6	179.3	1.98	32
BZ-12	62.8	29.9	178.6	1.93	41
BZ-13	62.9	29.6	179.9	1.96	36
BZ-14	62.9	29.7	185.7	2.01	26
BZ-15	62.6	30.2	196.5	2.12	8
BZ-16	63.1	30.7	196.6	2.05	20
BZ-17	63.1	30.4	191.4	2.01	26
BZ-18	63.3	29.1	188.7	2.06	18
BZ-19	63.1	29.4	181.7	1.98	33
BZ-20	61.9	27.2	142.0	1.74	76
BZ-21	63.4	31.4	162.2	1.64	93
BZ-22	62.8	30.1	156.0	1.67	87
BZ-23	62.8	28.3	167.1	1.91	45

TableA1 Specimen dimensions prepared for Brazilian tension test (cont.).

Specimen No.	Diameter (mm)	Length (mm)	Wight (mm)	Density (g/cc)	C%
BZ-24	62.7	29.4	162.7	1.79	65
BZ-25	63.0	30.6	170.4	1.79	67
BZ-26	62.6	29.6	165.4	1.82	61
BZ-27	62.9	28.8	157.7	1.76	71
BZ-28	63.0	28.0	154.4	1.77	70
BZ-29	62.7	29.5	162.2	1.78	68
BZ-30	62.5	29.4	160.2	1.78	68
BZ-31	62.9	30.0	165.1	1.77	69
BZ-32	62.8	27.7	167.2	1.95	38
BZ-33	63.4	28.0	180.0	2.04	22
BZ-34	63.0	29.0	176.0	1.95	38
BZ-35	61.8	28.6	178.2	2.08	15
BZ-36	62.6	28.8	149.3	1.69	85
BZ-37	62.8	29.3	162.6	1.79	66
BZ-38	62.8	28.6	148.3	1.67	87
BZ-39	62.9	28.0	161.7	1.86	54
BZ-40	63.0	29.0	159.8	1.77	70
BZ-41	61.7	30.0	150.2	1.68	87
BZ-42	62.8	28.9	150.1	1.68	86
BZ-43	47.4	23.7	89.3	2.14	0
BZ-44	47.4	23.7	85.4	2.04	0
BZ-45	47.4	23.7	97.8	2.34	0
BZ-46	62.8	31.3	207.2	2.14	0
BZ-47	62.7	31.0	203.9	2.13	0

TableA1 Specimen dimensions prepared for Brazilian tension test (cont.).

Specimen No.	Diameter (mm)	Length (mm)	Wight (mm)	Density (g/cc)	C%
BZ-48	62.9	30.8	201.6	2.11	0
BZ-49	62.7	33.4	217.5	2.11	0
BZ-50	62.7	32.5	209.6	2.09	0
BZ-51	62.7	30.8	199.2	2.10	0
BZ-52	62.1	30.6	201.3	2.17	0
BZ-53	62.0	30.7	200.7	2.17	0
BZ-54	62.4	32.0	202.4	2.07	0
BZ-55	62.3	30.7	202.1	2.16	0
BZ-56	62.2	30.1	199.7	2.18	0
BZ-57	62.2	30.4	197.7	2.14	0
BZ-58	62.0	30.7	200.4	2.16	0
BZ-59	62.7	32.1	217.5	2.20	0
BZ-60	63.1	32.3	211.3	2.09	0



TableA2 Specimen dimensions prepared for uniaxial compression testing.

Specimen No.	Width (mm)	Length (mm)	Height (mm)	Wight (mm)	Density (g/cc)	C%
UCS-01	54.6	53.8	108.9	526.8	1.65	92
UCS-02	54.6	55.2	110.9	623.5	1.86	53
UCS-03	54.5	53.8	110.6	656.0	2.02	24
UCS-04	51.9	49.1	107.4	423.0	1.61	100
UCS-05	54.6	54.9	111.3	569.8	1.71	81
UCS-06	55.0	56.9	107.4	547.0	1.63	95
UCS-07	53.4	53.5	110.4	559.0	1.77	69
UCS-08	54.2	54.7	109.7	590.8	1.82	61
UCS-09	55.8	56.2	110.1	646.8	1.87	51
UCS-10	52.9	53.4	101.8	500.5	1.74	75
UCS-11	53.9	54.3	107.7	561.3	1.78	68
UCS-12	57.0	55.8	110.7	633.3	1.80	65
UCS-13	50.3	53.6	111.2	517.5	1.73	78
UCS-14	54.9	53.4	107.6	600.0	1.90	46
UCS-15	53.4	53.7	108.0	582.3	1.88	50
UCS-16	53.3	56.0	109.5	625.0	1.91	44
UCS-17	52.8	55.7	111.0	541.0	1.66	90
UCS-18	55.2	55.3	109.2	720.3	2.16	0
UCS-19	53.9	53.2	108.9	565.0	1.81	62
UCS-20	55.0	55.7	107.7	694.0	2.10	0
UCS-21	53.1	54.9	107.8	665.3	2.12	0
UCS-22	55.3	56.3	110.0	599.5	1.75	73
UCS-23	55.0	55.3	110.2	577.8	1.72	78
UCS-24	56.3	53.5	105.8	621.5	1.95	37

TableA2 Specimen dimensions prepared for uniaxial compression testing (cont.).

Specimen No.	Width (mm)	Length (mm)	Height (mm)	Wight (mm)	Density (g/cc)	C%
UCS-25	53.9	53.4	106.5	563.5	1.84	57
UCS-26	54.5	54.7	110.0	541.5	1.65	91
UCS-27	55.6	56.2	110.5	609.8	1.77	70
UCS-28	51.0	52.1	106.1	536.3	1.90	46
UCS-29	53.5	52.6	104.7	460.8	1.56	106
UCS-30	54.0	53.6	108.4	581.0	1.85	55
UCS-31	55.5	55.9	110.2	711.3	2.08	14
UCS-32	53.5	54.8	109.7	586.3	1.82	60
UCS-33	57.9	54.1	109.8	639.6	1.86	54
UCS-34	55.0	54.8	110.3	633.4	1.91	45
UCS-35	54.3	54.6	110.4	554.0	1.69	84
UCS-36	54.8	54.1	109.6	641.6	2.06	19
UCS-37	55.6	54.9	110.0	567.0	1.69	84
UCS-38	56.1	57.2	111.6	619.4	1.73	77
UCS-39	57.5	56.8	110.5	604.4	1.67	87
UCS-40	55.1	55.9	110.4	574.9	1.69	84
UCS-41	53.4	53.6	109.5	667.3	2.13	5
UCS-42	53.3	53.4	109.1	664.5	2.14	0
UCS-43	52.8	53.7	109.2	665.7	2.15	0
UCS-44	55.2	56.0	109.2	742.6	2.20	0
UCS-45	53.9	56.0	108.8	702.8	2.14	0
UCS-46	55.0	55.3	109.5	703.2	2.11	9

TableA2 Specimen dimensions prepared for uniaxial compression testing (cont.).

Specimen No.	Width (mm)	Length (mm)	Height (mm)	Wight (mm)	Density (g/cc)	C%
UCS-47	53.1	53.2	107.8	642.6	2.11	9
UCS-48	55.3	55.7	107.8	700.1	2.11	9
UCS-49	55.0	54.9	109.0	687.4	2.09	13
UCS-50	56.3	56.3	109.2	727.1	2.10	11
UCS-51	53.9	55.3	108.8	675.0	2.08	14
UCS-52	54.5	53.5	108.8	662.8	2.09	13
UCS-53	55.6	53.4	109.0	679.8	2.10	11
UCS-54	51.0	54.7	109.5	650.7	2.13	5
UCS-55	53.5	56.2	108.6	692.2	2.12	7
UCS-56	57.9	52.1	109.1	704.3	2.14	4
UCS-57	55.0	52.6	109.1	675.7	2.14	4
UCS-58	54.3	53.6	109.1	679.9	2.14	4
UCS-59	54.8	55.9	109.0	710.9	2.13	5
UCS-60	55.5	55.1	109.0	713.8	2.14	0

TableA3 Specimen dimensions prepared for point load test.

Specimen No.	Diameter (mm)	Length (mm)	Wight (mm)	Density (g/cc)	C%
PL-01	64.0	38.5	252.1	2.04	22
PL-02	62.1	58.4	381.7	2.16	0
PL-03	89.0	41.0	491.7	1.93	41
PL-04	62.0	48.5	284.8	1.95	38
PL-05	62.0	69.3	452.6	2.16	0
PL-06	62.1	82.2	495.9	1.99	30
PL-07	60.5	53.4	308.9	2.01	26
PL-08	62.0	30.9	196.9	2.16	0
PL-09	81.6	117.0	1263.5	1.72	79
PL-10	61.7	58.4	356.3	2.06	17
PL-11	60.9	64.3	520.9	1.70	83
PL-12	60.4	84.0	809.0	1.81	62
PL-13	95.0	75.0	809.3	1.67	87
PL-14	53.3	53.7	268.5	1.65	92
PL-15	61.9	35.1	227.7	2.16	0
PL-16	62.2	72.9	480.2	2.16	0
PL-17	78.7	106.6	737.3	1.79	67
PL-18	54.1	70.8	342.1	1.64	92
PL-19	61.9	29.8	184.6	2.06	18
PL-20	64.2	64.6	355.0	1.62	97
PL-21	61.5	82.5	496.2	1.69	85
PL-22	61.0	40.6	557.9	1.87	51
PL-23	61.1	92.1	473.8	1.62	97

TableA3 Specimen dimensions prepared for point load test (cont.).

Specimen No.	Diameter (mm)	Length (mm)	Wight (mm)	Density (g/cc)	C%
PL-24	56.0	154.1	967.5	1.68	86
PL-25	53.1	54.4	205.7	1.92	42
PL-26	63.2	81.4	522.1	2.05	20
PL-27	62.6	88.0	451.6	1.60	100
PL-28	56.2	86.1	448.5	1.82	60
PL-29	58.0	54.4	489.3	1.91	44
PL-30	48.5	47.2	218.3	1.99	31
PL-31	52.2	77.7	370.4	1.69	84
PL-32	56.9	57.7	317.8	2.16	0
PL-33	66.2	69.0	445.0	1.77	69
PL-34	52.0	69.9	318.6	1.60	100
PL-35	52.0	51.4	272.0	1.96	35
PL-36	51.0	80.6	298.0	1.60	100
PL-37	49.1	53.0	465.7	1.62	96
PL-38	67.3	61.4	340.5	1.64	92
PL-39	56.0	54.5	329.0	2.00	29
PL-40	62.3	74.3	456.0	2.16	26
PL-41	62.1	72.5	383.2	2.16	74
PL-42	62.1	63.4	353.6	2.16	57
PL-43	63.1	75.1	490.0	2.16	13
PL-44	62.7	48.3	285.9	2.16	43
PL-45	62.5	62.5	383.5	2.16	28
PL-46	62.2	31.2	188.4	2.16	31
PL-47	63.2	32.1	163.8	2.16	95

TableA3 Specimen dimensions prepared for point load test (cont.).

Specimen No.	Diameter (mm)	Length (mm)	Wight (mm)	Density (g/cc)	C%
PL-48	62.2	80.1	495.8	2.16	22
PL-49	62.7	73.9	492.6	2.16	10
PL-50	62.1	74.1	458.6	2.16	21



TableA4 Specimen dimensions prepared for triaxial compression test.

Specimen No.	Width (mm.)	Length (mm.)	Height (mm.)	Wight (mm)	Density (g/cc)	C%
TRI-01	55.5	55.7	109.9	554.5	1.63	94
TRI-02	56.5	54.6	104.8	595.9	1.84	57
TRI-03	54.7	55.6	109.3	659.4	1.99	31
TRI-04	54.8	54.6	108.3	680.2	2.10	0
TRI-05	54.2	53.4	109.8	545.6	1.72	79
TRI-06	51.7	53.4	111.3	581.8	1.89	48
TRI-07	59.4	55.8	110.4	713.0	1.95	38
TRI-08	54.4	54.6	108.0	680.5	2.12	0
TRI-09	55.4	53.5	111.2	537.9	1.63	94
TRI-10	55.6	56.2	109.6	634.9	1.86	54
TRI-11	55.0	55.7	111.7	654.9	1.92	44
TRI-12	54.2	54.6	111.2	673.0	2.05	20
TRI-13	53.5	53.6	109.6	659.1	2.10	0
TRI-14	53.9	55.5	109.2	537.0	1.64	93
TRI-15	55.0	56.0	107.8	585.2	1.76	71
TRI-16	54.5	53.9	110.1	618.9	1.91	45
TRI-17	53.8	55.2	109.2	656.1	2.02	25
TRI-18	56.5	57.0	113.1	604.1	1.66	90
TRI-19	55.6	55.7	110.9	591.7	1.72	78
TRI-20	55.6	53.9	109.8	591.8	1.79	66
TRI-21	55.5	53.8	109.7	665.4	2.03	24
TRI-22	57.4	57.4	110.0	595.0	1.64	93
TRI-23	55.5	55.0	104.1	555.3	1.74	75
TRI-24	54.7	53.5	109.5	599.6	1.87	52

TableA4 Specimen dimensions prepared for triaxial compression test (cont.).

Specimen No.	Width (mm.)	Length (mm.)	Height (mm.)	Wight (mm)	Density (g/cc)	C%
TRI-25	53.5	54.5	111.3	655.1	2.01	26
TRI-26	56.5	54.6	104.8	657.1	2.16	0
TRI-27	55.6	56.2	109.6	535.0	2.16	0
TRI-28	56.5	57.0	113.1	583.2	2.16	0
TRI-29	55.6	55.7	110.9	616.9	2.16	0
TRI-30	54.7	53.5	109.5	654.1	2.16	0
TRI-31	56.5	54.6	104.8	602.1	2.16	0
TRI-32	59.4	55.8	110.4	589.7	2.16	0
TRI-33	55.0	55.7	111.7	589.8	2.16	0
TRI-34	54.5	53.9	110.1	634.9	2.16	0
TRI-35	53.8	55.2	109.5	537.0	2.16	0

BIOGRAPHY

Miss AmornratLuangthip was born on May 8, 1992 in BuriramProvince, Thailand. She received her Bachelor’s Degree in Engineering (Geotechnology) from SuranareeUniversity of Technology in 2015. For her post-graduate, she continued to study with a Master’s degree in the Geological Engineering Program, Institute of Engineering, Suranaree university of Technology. During graduation, 2015-2016, she was a part time worker in position of research assistant at the Geomechanics Research Unit, Institute of Engineering, Suranaree University of Technology.

